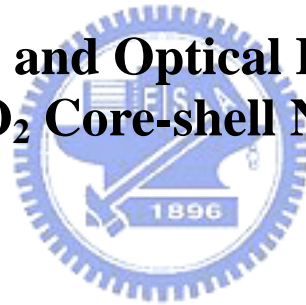


國立交通大學
電子工程學系電子研究所碩士班
碩士論文

一維氧化鋅/二氧化鈦核殼結構奈米線之光學與場
發射特性研究

**Field Emission and Optical Properties of 1D
ZnO/TiO₂ Core-shell Nanowires**



研究生：陳冠仲

指導教授：曾俊元

中華民國九十六年六月

一維氧化鋅/二氧化鈦核殼結構奈米線之光學與場
發射特性研究

**Field Emission and Optical Properties of 1D
ZnO/TiO₂ Core-shell Nanowires**

研究生：陳冠仲
指導教授：曾俊元 教授

Student: Guan-Zhong Chen
Advisor: Prof. Tseung-Yuen Tseng

國立交通大學
電子工程學系電子研究所碩士班
碩士論文

A Thesis

Submitted to Department of Electronics Engineering & Institute of

Electronics

College of Electrical and Computer Engineering

National Chiao Tung University

in partial Fulfillment of the Requirements

For the Degree of

Master

in

Electronics Engineering

June 2007

Hsinchu, Taiwan, Republic of China

中華民國九十六年六月

一維氧化鋅/二氧化鈦核殼結構奈米線之光學與 場發射特性研究


研究生：陳冠仲

指導教授：曾俊元

國立交通大學

電子工程學系 電子研究所

摘要



本論文主要探討以氧化鋅及二氧化鈦型成合殼結構奈米線，在低溫的環境中利用水熱法來形成氧化鋅奈米線當作核，再藉由濺鍍沉積法形成二氧化鈦殼層。藉由改變水熱法中的化學溶液濃度、成長時間來得到適當長度和密度的氧化鋅奈米線。再藉由改變濺鍍的溫度、時間和功率來得到均勻且不同厚度的二氧化鈦殼層，最後再利用濕式蝕刻法去除氧化鋅奈米線來製備空心二氧化鈦奈米管。並探討氧化鋅/二氧化鈦核殼結構奈米線的光學特性、晶體結構、表面型態及場發射特性，同時分析其加熱處理後對此結構的影響。


Field Emission and Optical Properties of 1D ZnO/TiO₂ Core-shell Nanowires

Student: Guan-Zhong Chen

Advisor: Tseung-Yuen Tseng

Department of Electronics Engineering and Institute of Electronics
National Chiao Tung University

Abstract

The logo of National Chiao Tung University is a circular emblem with a gear-like border. Inside the circle, there is a stylized building and the letters 'ES' and 'A' are visible. Below the building, the year '1896' is inscribed.

In this thesis, 1D ZnO/TiO₂ core-shell nanowires were prepared in two steps process. ZnO nanowires were fabricated by hydrothermal method at the low temperature as core. The ZnO nanowires were fabricated under the various solution concentrations and growth times of hydrothermal method in order to get a suitable ZnO nanowires array. TiO₂ shell was deposited by sputtering method under the various sputtering time and power to get a uniform and different thickness. TiO₂ tubes were fabricated by wet etching process. The optical properties, micro structure, surface morphology and the field emission characteristics of ZnO/TiO₂ core shell nanowires are studied. The structures after thermal treatment are also studied.

誌謝

首先誠摯的感謝指導教授曾俊元博士，老師悉心的教導使我得以一窺固態電子領域的深奧，不時的討論並指點我正確的方向，使我在這些年中獲益匪淺。老師對學問的嚴謹更是我輩學習的典範。

本論文的完成另外亦得感謝承佑、永昇和志洋學長的大力協助。因為有你們的意見和分析，使得實驗的過程中因而順利且完整。

兩年裡的日子，實驗室裡共同的生活點滴，學術上的討論、敗戰隊友遠征都不離不棄、義氣到底的革命情感、因為偷懶睡太晚而衝衝忙忙閃進實驗室.....，感謝眾位學長姐、同學、學弟妹的共同砥礪，你/妳們的陪伴讓兩年的研究生活變得絢麗多彩。

感謝家瑋、信賢、群傑、孟漢、聖裕等學長及秀玉和佳穎學姐的指導和費心，鎮宇、重毅、俊勝、俊興、士傑、松蒔和我共同努力及成長，以及毅函、世偉、啟翔和宏全你們的陪伴讓這兩年的研究生活變得絢麗多彩。

最後更感謝我的父母，默默地支持和栽培使我能完成這段歷程，這份喜悅禮是屬於你們的。

Contents

Chinese Abstract	I
Abstract	II
Acknowledgement	III
Contents	IV
List of Illustrations	VI
List of Tables	IX
Chapter 1 Introduction	1
1.1 Nanostructures	1
1.2 ZnO Characteristics	2
1.2.1 The Growth Methods of ZnO Nanowires	3
1.2.2 The Optical Properties.....	7
1.3 TiO ₂ Characteristics	12
1.4 Core-shell Structures	14
1.5 Field-Emission Properties.....	16
Chapter 2 Experiment Details	18
2.1 The Process Flow of Experiment	18
2.2 Sample Preparation.....	19
2.2.1 Wafer Clean.....	20
2.2.2 Deposition of ZnO Seed Layer	20
2.2.3 Growth ZnO Nanowires Array.....	22
2.2.4 Synthesized of ZnO/TiO ₂ Core-shell Structures	23
2.2.5 Synthesized TiO ₂ Nanotubes.....	24
2.3 Measurement Equipment.....	25
2.3.1 Field Emission Scanning Electron Microscopy (FE-SEM).....	25
2.3.2 High Resolution Transmission Electron Microscopy (HR-TEM) and Dispersive X-Ray Energy (EDX).....	26
2.3.3 X-Ray Diffraction (XRD)	26
2.3.4 Ultraviolet-Visible Spectrophotometers.....	27
2.3.5 Cathodluminescence (CL).....	28
2.3.6 Field Emission Detector	29
Chapter 3 Results and Discussion	30
3.1 ZnO Aeeding Layer	30
3.1.1 The Field Emission Scanning Electron Microscopy Analyses .	32
3.1.2 The X-Ray Diffraction Analyses	33
3.1.3 Ultraviolet-Visible Spectrophotometers Analyses.....	34

3.2 ZnO Nanowires.....	35
3.2.1 Characterization of ZnO Nanowires	36
3.2.2 The Optical Properties.....	42
3.2.3 The Field Emission Properties	45
3.3 ZnO/TiO ₂ Core-shell Nanowires	49
3.3.1 The Field Emission Scanning Electron Microscopy Analyses ..	49
3.3.2 The High Resolution Transmission Electron Microscopy and Dispersive X-Ray Energy Analyses.....	53
3.3.3 The X-Ray Diffraction Analyses	56
3.3.4 The Optical Properties.....	59
3.3.5 The Field Emission Properties	62
3.4 TiO ₂ Nanotubes.....	67
3.4.1 The Field Emission Scanning Electron Microscopy analyses ..	67
3.4.2 The High Resolution Transmission Electron Microscopy Analyses and Dispersive X-Ray Energy	68
Chapter 4 Conclusions	74



List of Illustrations

Figure 1-1. Wurtzite structure of ZnO.	2
Figure 1-2. VLS process.	4
Figure 1-3. The schematic geometry of ZnO nanowires growth. 1. Furnace tube, 2. slender tube, 3. source, 4. template, 5. alumina supporter	4
Figure 1-4. The growth process of the ZnO nanowires by the hydrothermal method.	6
Figure 1-5. The mechanism of the photoluminescence.	8
Figure 1-6. The draft of the calculated defect's levels in ZnO film.	9
Figure 1-7. Schematic showing the energy-band diagram of a ZnO grain in cross section. The conduction band (E_c), valance band (E_v), Fermi level (E_F), paramagnetic oxygen vacancy (V_O^*) level, and the diamagnetic V_O^{**} area (hatched) in the grain-boundary depletion region are visualized for a grain with a (a) low and (b) high free-carrier density. The circles and arrows symbolize electron-hole recombination events which emit green light.	11
Figure 1-8. Band bending of nanowires.	16
Figure 2-1. The structure of ZnO nanowires array.	22
Figure 2-2. The structure ZnO/TiO ₂ core-shell.	23
Figure 2-3. TiO ₂ nanotubes was fabricated by wet-etching (a) 30 min (b) 60 min.	24
Figure 2-4. Schematic diagram of a high-vacuum chamber system for field emission property measurement.	29
Figure 3-1. SEM image of ZnO nanoflowers.	31
Figure 3-2. The SEM image of ZnO seeding layer on the Si substrate. (a) Top view (b) cross section.	32
Figure 3-3. XRD patterns of ZnO seeding layer on Si substrate as deposition and after thermal annealing at 750°C 3 hours.	33
Figure 3-4. The transmittance spectra of ZnO seeding layer.	34
Figure 3-5. The pourbaix diagram of the Zn(OH) ₂ .	35
Figure 3-6. The SEM image ZnO nanowires grew in (a) 0.5 M (top view) (b) 0.5 M (cross section) (c) 0.1 M (top view) (d) 0.1 M (cross section) (e) 0.05 M (cross section) (f) 0.025 M (cross section) (g) 0.0125 M (top view) (h) 0.0125 M (cross section) (i) 0.01 M (cross section).	38

Figure 3-7. Aspect ratio of ZnO nanowires as a function of concentration.	38
Figure 3-8. (a) Cross-section FE-SEM micrographs of ZnO nanowires at 0.0125 M with growing 60min (b) 75 min (c) 90 min (d) 105 min (e)120 min (f) 150 min (g) 180 min.	40
Figure 3-9. Average length of ZnO nanowires as a function of growth time.	41
Figure 3-10. The X-ray diffraction pattern of ZnO nanowires grown on Si wafer with different growth time (a) 70 min (b)120 min.	41
Figure 3-11. The CL spectra of ZnO nanowires for 70min and 120 min.	43
Figure 3-12. The CL spectra of ZnO nanowires as growth and after annealing.	44
Figure 3-13. Field emission current-voltage curves of ZnO nanowires with different growth time.	46
Figure 3-14. The Fowler-Nordhiem (F-N) plots of ZnO nanowires with different growth time	47
Figure 3-15. SEM images of ZnO/TiO₂ core-shell nanowires deposited at room temperature.	50
Figure 3-16. SEM images of ZnO/TiO₂ core-shell nanowires with different sputter arameters.	52
Figure 3-17. The TEM micrographs of (a) ZnO/TiO₂ core-shell structure. (b) region A (c) region B (d) region C. (e) The HR-TEM micrographs of region A (d) SAED spectra of region A.	54
Figure 3-18. The XRD patterns of ZnO/TiO₂ core-shell structure with various sputtering power, time (a) as TiO₂ deposition, (b) after annealing 400°C 1 hour in air, (c) after annealing 500°C 1 hour in air.	58
Figure 3-19. CL spectra of ZnO nanowires and ZnO/TiO₂ core-shell nanowires as deposited.	60
Figure 3-20. (a) CL spectra of ZnO nanowires and ZnO/TiO₂ core-shell nanowires after annealing 400°C (b) 500°C 1 hour under the air.	61
Figure 3-21. Schematic energy level diagram of a ZnO/TiO₂ core-shell structure.	62
Figure 3-22. (a) Field emission current-voltage curves of ZnO/TiO₂ core-shell nanowires as deposited. (b) The F-N plot of ZnO/TiO₂ core-shell nanowires as deposited.	63
Figure 3-23. (a) Field emission current-voltage curves of ZnO/TiO₂ core-shell nanowires after annealing. (b) The F-N plot of ZnO/TiO₂	

core-shell nanowires after annealing.	65
Figure 3-24. The SEM image of ZnO/TiO ₂ core-shell nanowires after wet etching 30 min (a) top view (b) cross section.	68
Figure 3-25. The TEM micrographs of (a) TiO ₂ tube. (b) region B (c) SAED spectra of region B.	70
Figure 3-26. The TEM micrographs of (a) ZnO/TiO ₂ nanowire. (b) region B.	72
Figure 3-27. SAED spectra of (a) region B (b) region C.	73



List of Tables

Table 1-1. Typical physical and mechanical properties of titania.	12
Table 3-1. The detail data of field emission property of ZnO nanowires with different growth time.	48
Table 3-2. The atomic percentage of ZnO/TiO₂ core-shell structure analyses by EDX.	55
Table 3-3. The detail data of field emission property of ZnO/TiO₂ core-shell nanowires as deposited.	64
Table 3-4. The detail data of field emission property of ZnO/TiO₂ core-shell nanowires after annealing.	66
Table 3-5. The atomic percentage of ZnO/TiO₂ core-shell structure analyses by EDX.	70
Table 3-6. The atomic percentage of ZnO/TiO₂ core-shell structure analyses by EDX.	73



Chapter 1 Introduction

1.1 Nanostructures

Recently, nanotechnology had been research extensively. Nanostructures can be defined as systems in which at less one dimension is smaller than 100 nm where new physical, chemical and biological properties occur as compared to bulk materials. There are many kinds of nanostructure, including one dimension (1D) nanostructure such as nanowire¹, nanotube²³⁴, nanorods⁵⁶⁷; two dimension (2D) nanostructure such as nanoblet⁸, nanosheets^{9 10}, nanoplanes; three dimension (3D) nanostructure such as nanoflower¹¹, tetrapod nanorod¹², nanoparticle¹³. Because of the specially electronic and optical properties of nanostructures they have high potential in application of the electron and optical devices. For example, nanodot was applied in nonvolatile memory, nanorods in field emission, nanowires in solar cell, etc.

Since the carbon nanotubes (CNTs) were discovered in 1991¹⁴, the one dimension (1D) nanostructures were attracted a lot of attention. Except carbon, many materials were researched to use in nanodevices, like ZnO, GaAs and TiO₂ etc. The III-V group semiconductor are always used for light emitting diodes (LED), and ZnO are used for ultraviolet (UV) laser devices, field emission display, solar cell etc.

The subject is focused on characteristic and fabrication of 1D ZnO nanostructures and ZnO/TiO₂ core-shell nanostructures.

1.2 ZnO Characteristics

Zinc oxide (ZnO) is a II-VI group semiconductor, has a stable wurtzite structure (Figure 1-1) with lattice spacing $a = 0.325$ nm and $c = 0.521$ nm. The ratio of c/a is 1.633 which is nearly perfect. It has high melting point (1975°C) and high thermal stability. Its molecular mass is 81.39. Its specific heat is 0.125 cal/gm. And its thermal conductivity is 0.006 cal/cm/K. ZnO is a wide band gap semiconductor (3.37eV) with a large exciton binding energy (60meV) at room temperature, and is one of the most important and versatile semiconductor materials. Previous studies were investigated into its optical and electric properties, as well as its ferromagnetic, transparency, photoconductivity, piezoelectric, field emission, and light-emitting properties. Further, ZnO has attracted much attention since possible applications in phosphors, transparent conducting films for solar cells¹⁵, ultra-violet (UV) laser devices¹⁶ and flat panel displays¹⁷ were suggested.

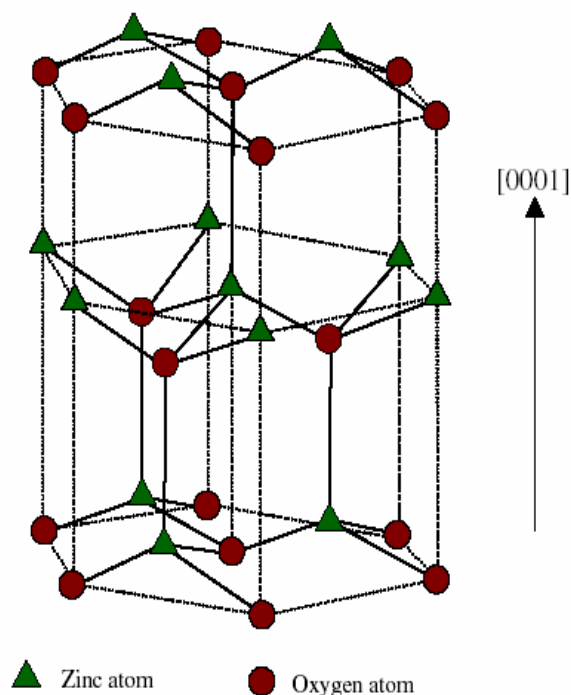
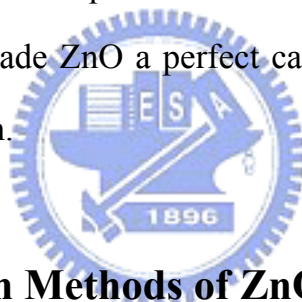


Figure 1-1. Wurtzite structure of ZnO.

Since the first report of ultraviolet lasing from ZnO nanowires, nanostructure of ZnO has stimulated intensive research. Indeed, ZnO nanostructures are interesting to study not only the property of UV lasing emission in nanowire form, but also because a wide variety of morphologies have been prepared. Some kinds of the ZnO nanostructures contain nanowire, nanorod, nanosheet, nanoribbon, nanotube, nanoplate, tetrapod, and flower-liked structures. Indeed, based on the nano-scale structure on interface, those applications of morphological properties will exceed normal expectations and behave prominent effect.

Moreover, the high melting point, excellent chemical stability and small electron affinity which are the requirements to be an ideal anode material for field emission (FE) have made ZnO a perfect candidate for carbon nanotubes (CNTs) in the field emission.



1.2.1 The Growth Methods of ZnO Nanowires

There are a lot of methods of synthesizing ZnO nanowires such as VLS (vapor-liquid-solid) method, metal-organic chemical vapor deposition, thermal evaporation, electro-chemical deposition, template enhancement method, and hydrothermal method.

VLS (vapor-liquid-solid) method

The VLS (vapor-liquid-solid) process was originally developed by Wagner and Ellis to produce micrometre-sized whiskers during the 1960s¹⁸. In a typical VLS process, ZnO powder and graphite were milled appropriately and loaded into an alumina boat, then placed the boat in the center of a quartz tube under N₂ and Ar flow as the carrier gas. As the temperature is increased to the

reaction temperature, the ZnO react with graphite to form Zn(g) and CO(g). The gaseous products produced by reactions (1) and (2) would adsorb and condense on the metal catalytic droplets. And then followed by nucleation and growth of single crystalline ZnO nanowires (Figure 1-2) following by the reaction (3). The corresponding chemical reaction can be shown in Figure 1-3.

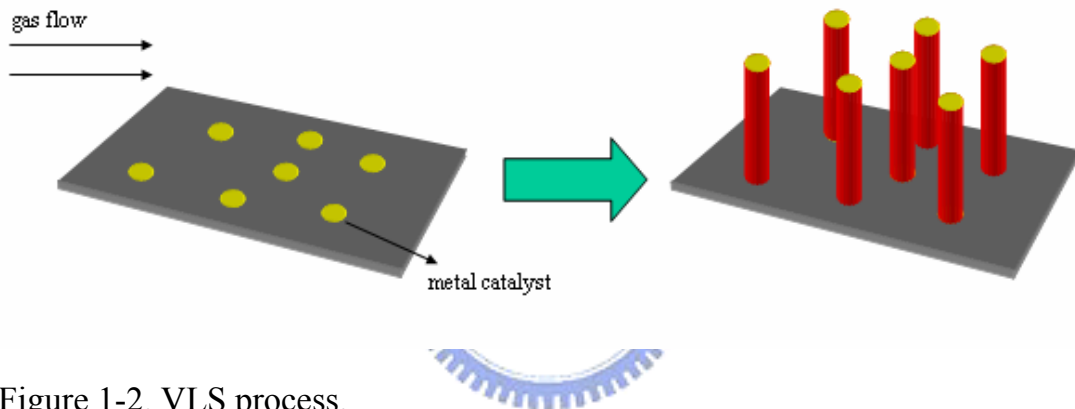
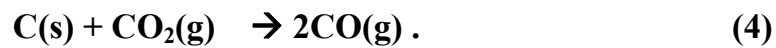
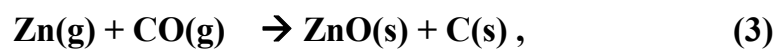
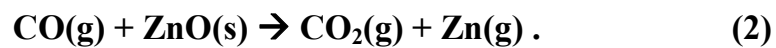
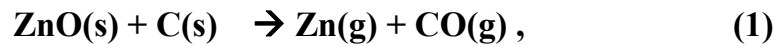


Figure 1-2. VLS process.



Figure 1-3. The schematic geometry of ZnO nanowires growth. 1. Furnace tube, 2. slender tube, 3. source, 4. template, 5. alumina supporter

Various vapor-phase methods such as the vapor-liquid-solid epitaxial (VSLE), pulsed laser deposition (PLD), and metal-organic chemical vapor deposition (MOCVD) have been successfully used to grow oriented ZnO

nanowire arrays at temperatures of 800-900°C. In order to lower the temperature of the growing process, the ZnO nanowire can dope some impurities like tin (Sn) and indium (In). It can low the temperature of the growth about 500-600°C. The VLS (vapor-liquid-solid) method needed catalysts like aurum (Au) and copper (Cu). The control of the flow rate was very important. It affected the length, diameter and the density of the ZnO nanowires.

The template method¹⁹

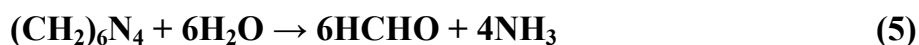
The template method is that the porous Anodic Aluminum Oxide (AAO) substrate was used as a template to synthesize the ZnO nanowires. The AAO structure would provide some properties for nanowires, including high pores density, controllable diameter and length of pores, large area and high uniform. It can use many methods like CVD, sol-gel and hydrothermal method to fill the hole of the AAO template. After filling the ZnO, use NaOH solution to remove the AAO template and the ZnO nanowires remain on the substrate. It is easy and cheap to synthesize ZnO nanowires, but it has impurity problems and hard to create single crystal ZnO nanowires.

The hydrothermal method^{20,21,22}

The hydrothermal method was the cheapest method to grow ZnO nanowires. It has some advantages over other growth processes such as catalyst-free growth, low cost, large area uniform production, environmental friendliness, and low reaction temperature (below 100°C) to integrate into the microelectronics and plastic electronics.

The ZnO seeding layer which can help ZnO nanowires grow along

C-orientation was put into an aqueous solution of the zinc nitrate hexahydrate ($\text{Zn}(\text{NO}_3)_2 \cdot 6\text{H}_2\text{O}$ (99.9% purity)) and the hexa-methylenetetramine (HMTA; $\text{C}_6\text{H}_{12}\text{N}_4$, (99.9% purity)) in a sealed vessel. Zinc nitrate hexahydrate is used as source of zinc and hexamethylenetetramine is used to control the PH value. These can be represented by the following reactions:



The hydrothermal method is involved two steps as nucleation and growth. When zinc nitrate hexahydrate and hexa-methylenetetramine are mixed together, no precipitation accrues initially. With the increase of temperature, the HMTA begins to decompose into ammonia and then $\text{Zn}(\text{OH})_2$ occurred. The precipitation appeared quickly. And then ZnO nuclei are formed on the substrate. After the ZnO film grows from the nuclei, the ZnO nanowires begin to grow. The growth process is shown in Figure 1-4.

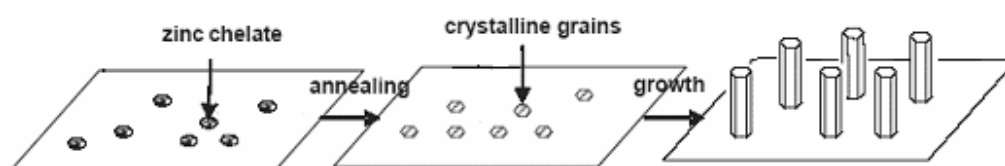


Figure 1-4. The growth process of the ZnO nanowires by the hydrothermal method.

So the synthesis of one-dimensional ZnO nanostructures by wet chemical approach without involving catalysts or templates provides a promising option

for the large-scale production of well-dispersed one-dimensional nanostructured materials .

1.2.2 The Optical Properties

Recently, ZnO have been used in optical application widely, such as ultraviolet laser. ZnO is a well-known semiconductor for its wide band gap and high exciton binding energy at room temperature.

The strong exciton binding energy of ZnO (~ 60 meV) is much larger than that of ZnSe (~ 22 meV) and GaN (~ 25 meV), also larger than the thermal energy of ZnO (~ 26 meV), which are favorable for obtaining an efficient excitonic laser action at room temperature. So ZnO is a good candidate for blue-UV emission optoelectronic devices.

Zinc oxide (ZnO) generally had two kinds of emission manner. One was the ultraviolet emission, the other was the green emission. The ultraviolet emission was related to the exciton emission of ZnO. The mechanism of the emission is shown in Figure 1-5. The green emission was related that the electron transition from valence band to the energy band of impurity. If the component, structure and defects changed, the characterization of emission changed²³.

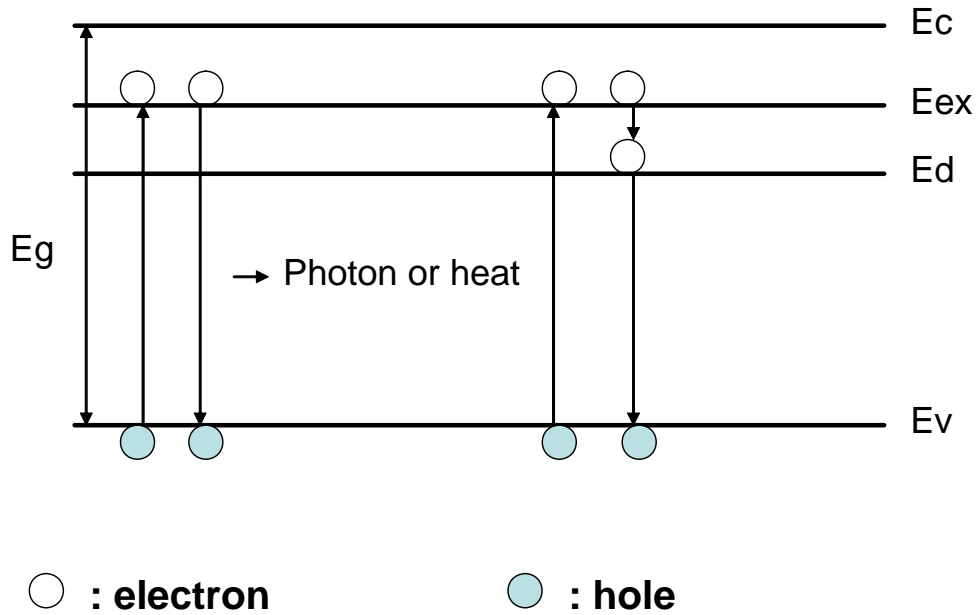


Figure 1-5. The mechanism of the photoluminescence.

The green emission²⁴ (519 nm) originates from the oxygen vacancies according to the result of Vanheusden et al.²⁵. By full-potential linear muffin-tin orbital method, the green emission of ZnO is because that the oxygen interstitials (O_i) occupy the zinc vacancies (V_{Zn}) to form the defect of antisite oxide (O_{Zn}). The kind of defect is easily formed because the antisite oxide has relatively low formation energy. It is shown in Figure 1-6. All the prepared films are n-type and the majority donors are oxygen vacancies (V_O) and zinc interstitials (Zn_i). It is proved that the singly ionized oxygen vacancy is responsible for the green emission and this emission results from the recombination of a photogenerated hole with a singly ionized charge state of this defect. The more singly ionized oxygen vacancies there are, the stronger the luminescence intensity is.²⁶

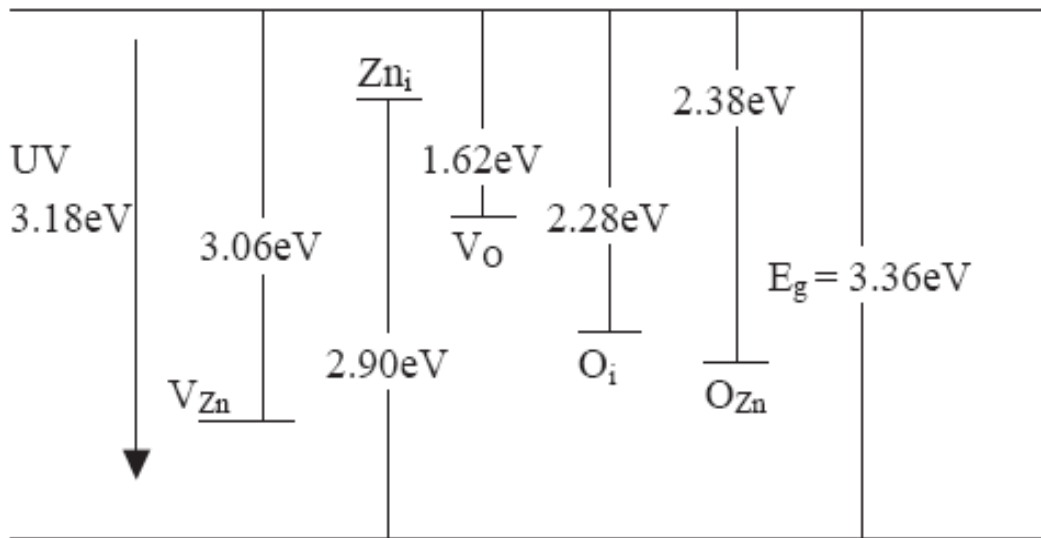


Figure 1-6. The draft of the calculated defect's levels in ZnO film.

The mechanism of the photoluminescence is that the photon excited the electrons from valence band to excited state of ZnO. And then electrons and holes recombine together to release the photon, heat or another form of energy. The exciting energy must be higher than the energy level of ZnO. The illuminant energy is absorbed by electrons of the sample and then electrons will jump to higher level. After that it would spontaneously jump to the low level. And then release the energy in the form of light. When there exists another energy state between excited state and the valence band, for example: donor level or acceptor level. The electrons jump from the valence band to the excited state and then jump from the excited state to donor level or acceptor level and the last to the valence band. Besides, as the carrier concentration increases, the excited state would approach the conduction band. At last, it would form the degeneration phenomenon. The number of the defects may affect the luminescence efficiency very much. When the electron is excited to the excited state, if there are too many defects between the excited state and the valence band, the electron is easy to be absorbed by the defect, the part electrons can

not recombine with the holes in the valence band. So they make luminescence efficiency reduce and influence the power of intensity.

Oxygen vacancies in ZnO can occur in three different charge states : the V_{ϕ} state which has captured two electrons and is neutral relative to the lattice, the singly ionized V_{O}^{*} state, and the V_{O}^{**} state which did not trap any electron and is doubly positively charged with respect to the lattice. The V_{ϕ} state is assumed to be a very shallow donor²⁷. The description is shown in Figure 1-7.



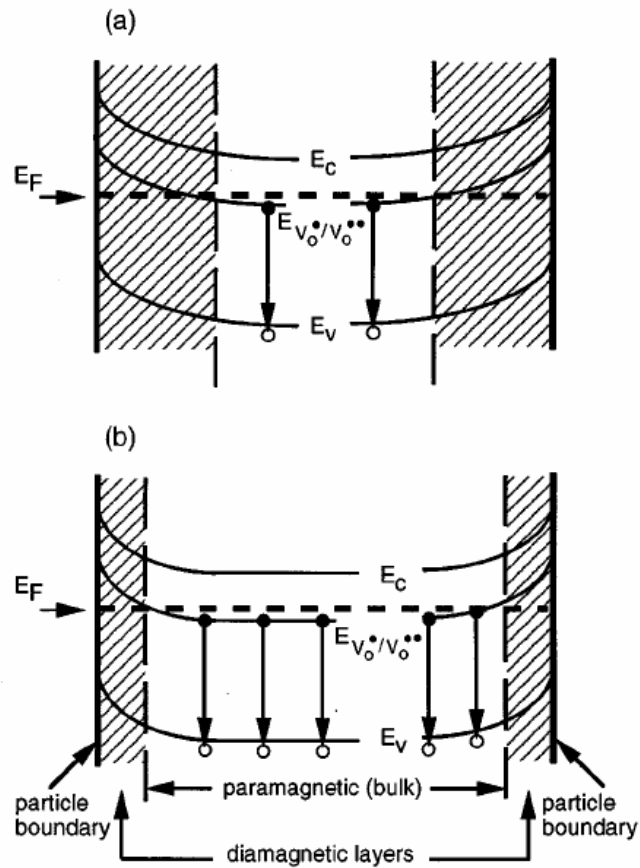


Figure 1-7. Schematic showing the energy-band diagram of a ZnO grain in cross section. The conduction band (E_C), valence band (E_V), Fermi level (E_F), paramagnetic oxygen vacancy (V_O^*) level, and the diamagnetic V_O^{**} area (hatched) in the grain-boundary depletion region are visualized for a grain with a (a) low and (b) high free-carrier density. The circles and arrows symbolize electron-hole recombination events which emit green light.

1.3 TiO₂ Characteristics²⁸

Titanium dioxide, also known as titanium (IV) oxide or titania, is the naturally occurring oxide of titanium, chemical formula TiO₂. Titanium dioxide exists in a number of crystalline forms including Rtile, Aatase, Bookite, Titanium dioxide (B) or TiO₂(B). Rtile and Aatase are most important crystalline forms in the electronic industry. There are physical and mechanical properties of TiO₂ in the Table 1-1.

Density	4 gcm ⁻³ Anatase : 3.84 gcm ⁻³ Rtile : 4.26 gcm ⁻³
Porosity	0%
Modulus of Rupture	140MPa
Compressive Strength	680MPa
Poisson's Ratio	0.27
Fracture Toughness	3.2 Mpa.m ^{-1/2}
Shear Modulus	90GPa
Modulus of Elasticity	230GPa
Microhardness (HV0.5)	880
Resistivity (25°C)	10 ¹² ohm.cm
Resistivity (700°C)	2.5x10 ⁴ ohm.cm
Dielectric Constant (1MHz)	85
Dissipation factor (1MHz)	5x10 ⁻⁴
Dielectric strength	4 kVmm ⁻¹
Thermal expansion (RT-1000°C)	9 x 10 ⁻⁶
Thermal Conductivity (25°C)	11.7 WmK ⁻¹
Refractive Index	Anatase : 2.46 Rtile : 2.903
Crystal Structure	Anatase : Tetragonal Rtile : Tetragonal

Table 1-1. Typical physical and mechanical properties of titania.

Nanosized titanium dioxide (TiO₂) structures have been the subject of a great deal of research because of their unique physicochemical properties and

applications in the areas of pigments²⁹, gas sensors, catalysis, photocatalysts³⁰, photovoltaics³¹, optics, inorganic membranes, field emission³² and dielectric materials. It is not surprising in view of the importance of TiO₂ nanostructures that a wide variety of approaches for the synthesis of nanosized TiO₂ have been reported, and it remains a particularly active research field.



1.4 Core-shell Structures³³

In recent years, there has been interest surrounding the fabrication of core-shell structures that consist of templated cores coated with shells of different chemical composition. These core-shell structures often exhibit properties that are different from those of the templated cores (for example, increased stability, higher surface area, and different magnetic and optical properties), thus making them attractive from both scientific and technological viewpoints³⁴. Furthermore, the properties of core-shell particles can be also tailored in a controllable fashion by independently altering the composition, dimension, and structure of the core or shell. Applications for such core-shell spheres are diverse, including solar cell³⁵, optical resonance engineer³⁶, photonic crystal³⁷, biosensor³⁸, etc.

In general there are many kind methods to synthesize nanosize core-shell structures the most important of which are polymer, inorganic and biomacromolecule coating methods. Now we focus of the inorganic coating methods. At 2006s, Chen et al.¹¹ has succeed to synthesize the amorphous titania-coated zinc oxide nanoparticles core-shell structures by two step process. First, ZnO nanoparticles were prepared by the solvothermal synthesis in ethanol. And then ZnO nanoparticles were coated with amorphous TiO₂ via a sol-gel process. And they reported that TiO₂ shell thickness on the surface of ZnO nanoparticles was very important in the enhancement of PL intensity. At 2005s, Zheng et al.¹² had fabricated T-ZnO/SnO₂ core-shell nanorods. Zinc powder was heated on the silicon wafer with oxygen flow to prepare the T-ZnO nanorods. The as-grown T-ZnO nanorods was heated to the desired temperature (typically T = 770 °C) with SnH₄/N₂ flow. The products,

T-ZnO/SnO₂ core-shell heterostructures were accomplished. At 2006s, Yang *et al.*³⁵ used ZnO-Al₂O₃ and ZnO-TiO₂ Core-Shell Nanowire to synthesize dye-sensitized solar cells. They grew ZnO nanowires as the core by hydrothermal method. Shells of Al₂O₃ or TiO₂ were deposited on the nanowires films by atomic layer deposition (ALD) process.



1.5 Field-Emission Properties

It is well known that high aspect ratio and sharp tip nanostructures like nanowires, nanotubes and nanorods are suitable for cold cathode field emission application. When negative voltage was applied on nanowires, the negative voltage would induce a high electric field on the tip of structures. The high electric field will let the potential barrier narrow as shown in the Figure 1-8. If the potential barrier is narrow enough, electrons would pass through the barrier as a result in the current.

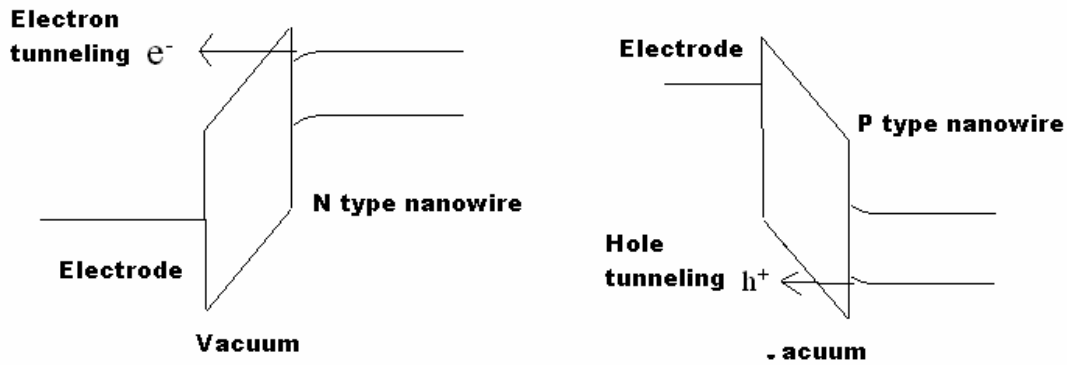


Figure 1-8. Band bending of nanowires.

This phenomenon we also know as Fowler-Nordheim tunneling. This phenomenon is highly dependent on both properties of the material and the shape of the particular cathode, so that higher aspect ratios produce higher field emission currents. This field emission current density can be described by the F-N equation. The F-N equation is as follows:

Fowler-Nordheim (F-N) equation :

$$J = \frac{A\beta^2 E^2}{\Phi} \exp\left[-\frac{B\Phi^{\frac{3}{2}}}{\beta E}\right] \quad [1.1]$$

$$A = 1.56 \times 10^{-10} (AV^{-2}eV) \quad [1.2]$$

$$B = 6.83 \times 10^3 (eV^{-\frac{3}{2}}V/um) \quad [1.3]$$

Where J is the current density, E is the applied electric field of tip, Φ is the work function (ev), β is the field emission enhancement factor, A and B are constants. The logarithmic form of Eq. [1.1] can be expressed as follow:

$$\ln\left(\frac{J}{E^2}\right) = -\frac{B\Phi^{\frac{3}{2}}}{\beta} \frac{1}{E} + \ln\left(\frac{A\beta^2}{\Phi}\right) \quad [1.4]$$

A plot of $\log(J/E^2)$ versus $1/E$ will be a straight line with slop m and intercept b. Slop m and intercept b is given by follow:

$$m = -\frac{B\Phi^{\frac{3}{2}}}{\beta} \quad [1.5]$$

$$b = \ln\left(\frac{A\beta^2}{\Phi}\right) \quad [1.6]$$

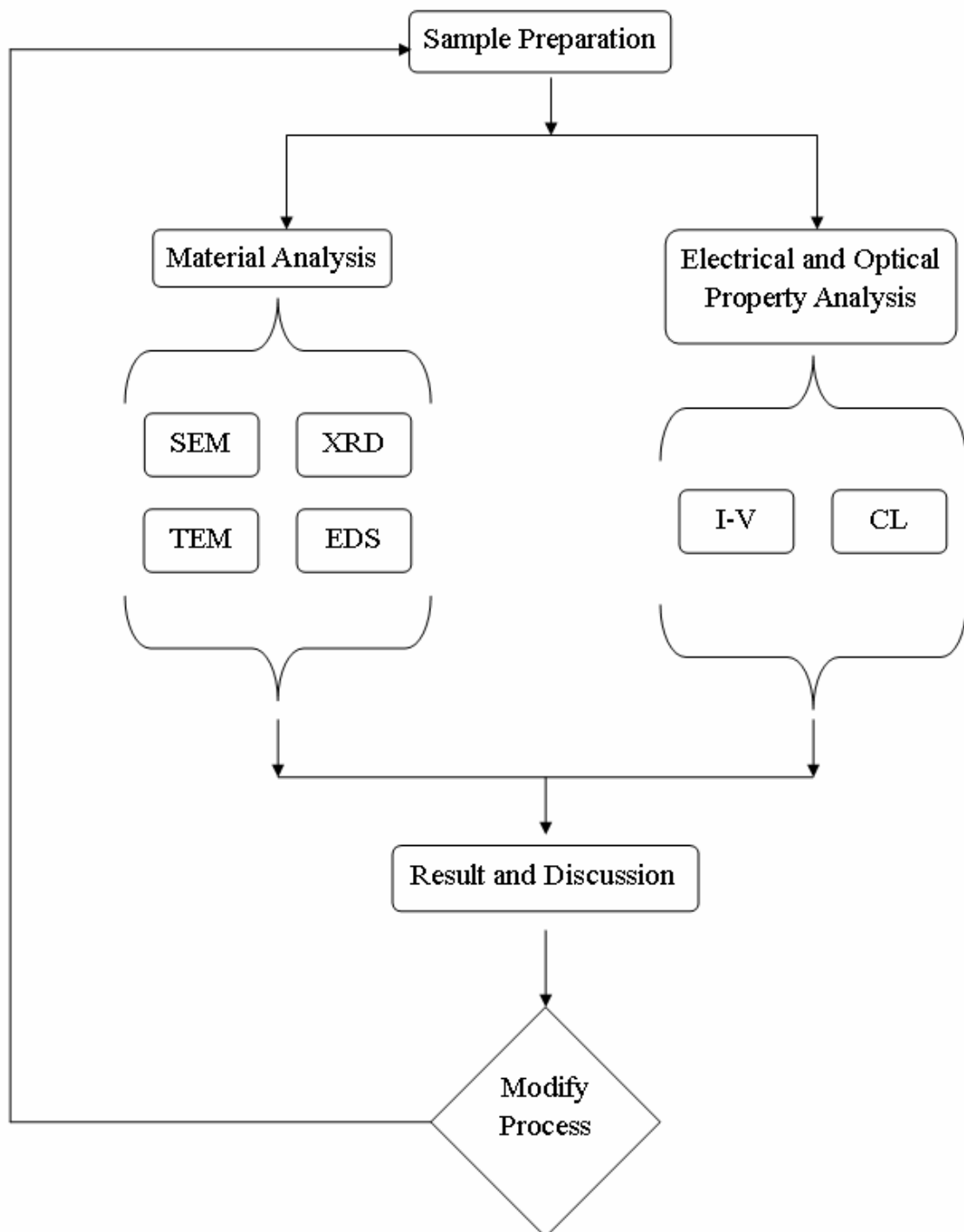


The value β can be calculated by the F-N plot. The β value presents the field emission effect well or not. In other words high β value represents a strong field emission mechanism; low β value means a poor field emission mechanism. Besides, it is well know that the β value only depends on geometry, structure, tip size and number of emitters on substrate.

Chapter 2 Experiment Details

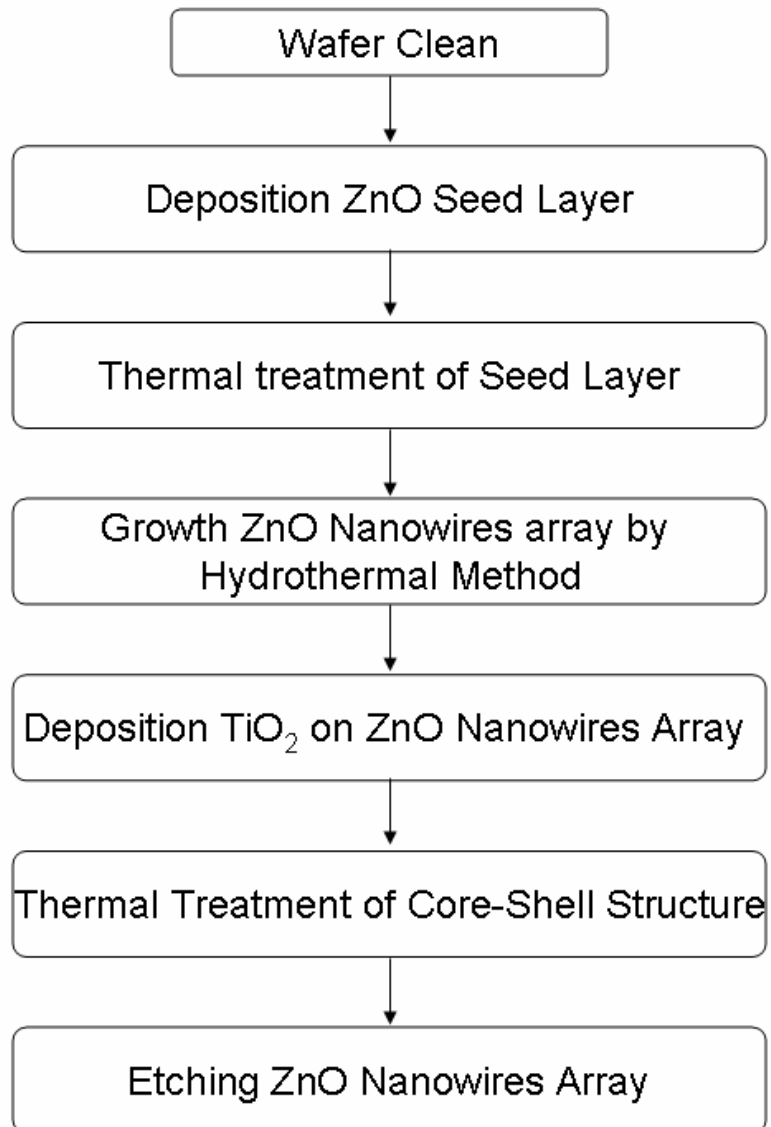
2.1 The Process Flow of Experiment

Flow chart of experiment



2.2 Sample Preparation

Flow chart of sample preparation



2.2.1 Wafer Clean

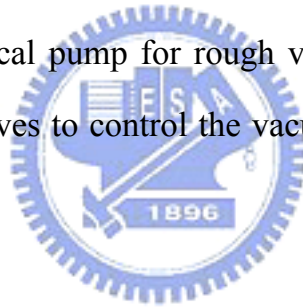
In the experiment, the p-type Si (100) substrate was cleaned by a standard Radio Corporation of America (RCA) cleaning method and rinsed in acetone for 30 min. to remove native oxide from the surface of Si substrate.

2.2.2 Deposition of ZnO Seed Layer

The ZnO seed layer which can help to grow well-aligned ZnO nanowires was deposited by Radio frequency (RF) magnetron sputtering system. The Sputtering system can be divided into five parts.

Vacuum system:

It contains a mechanical pump for rough vacuum, a diffusion pump for high vacuum, and three valves to control the vacuum pressure in chamber and in tubes.



Pressure system

There are two digital gauges in pressure system. One is Granville-Phillips Co.'s product, which provides an accuracy of 0.1m torr with a display range from 1 ATM to 0.1m torr to show the chamber pressure condition for low vacuum. And the other is an ion gauge, which would show the pressure condition of high vacuum from 10^{-3} to 10^{-7} torr. Accordingly, we can monitor the vacuum situation in sputter chamber under sputtering, through these two machines.

Gas flow controlling system

Generally speaking, the content of oxygen plays an important role in oxide ceramics. So we utilize Gas MFC (mass flow meter) to control the flow rate and atmosphere ratio during thin film deposition process in order to examine the atmosphere ratio dependence.

Plasma controlling system

We set the system, which involves a RF power generator, an automatic network-matching box, a 2-inch magnetron gun and its shutter and 2-inch one to produce plasma. The power generator can provide the maximum power of 600 W (13.56MHz), besides, the automatic network-matching box can adjust the capacitances of the total network for minimum reflection power. Consequently, we are able to adjust the power magnitude to modify our process.



Cooling system

The recurring water circling sputter machine is driven by pump for cooling all system.

The ZnO seeding layer was deposited on Si wafer under 10 mtorr Argon (Ar) and Oxygen (O₂) flow ratio 3:1 using home made ZnO target with 30W for 30 min. After deposited the sample was put into the oven for in-situ annealing at 750°C for 3 hours under Ar flow 30 sccm. The thickness of the ZnO seeding layer was about 600 Å. The epitaxial ZnO seeding layer had a dominant orientation along (002). The pure ZnO target was made by the ZnO powders (99.7%). The ZnO powders were first dry ball-milled for thirty minutes and wet ball-milled in alcohol for 24 hours to ensure the powders were uniform. After the milling, put the binder into the ZnO powders and mill again.

After the milling, put it in the 2.5 inch pattern and press the pattern to 15000 p.s.i. for 1 min. Finally, the stressed powders were put into the oven to sinter at 1300°C for 4 hours. After sintering, grind the target into 2 inch in diameter. Then plaster the ZnO target and copper plate with Ag glue and put into the oven to sinter for 1 day.

2.2.3 Growth ZnO Nanowires Array

The Si substrate with ZnO seeding layer was put into an aqueous solution of zinc nitrate hexahydrate ($\text{Zn}(\text{NO}_3)_2 \cdot 6\text{H}_2\text{O}$, (99.9%)) and hexamethylenetetramine (HMTA ; $\text{C}_6\text{H}_{12}\text{N}_4$, (99.9 %)) in a sealed vessel at 95 °C for various reaction times from 10 min to 150 min. The concentration of zinc and amine were fixed at 0.0125 M. The structure was as below (Figure 2-1).

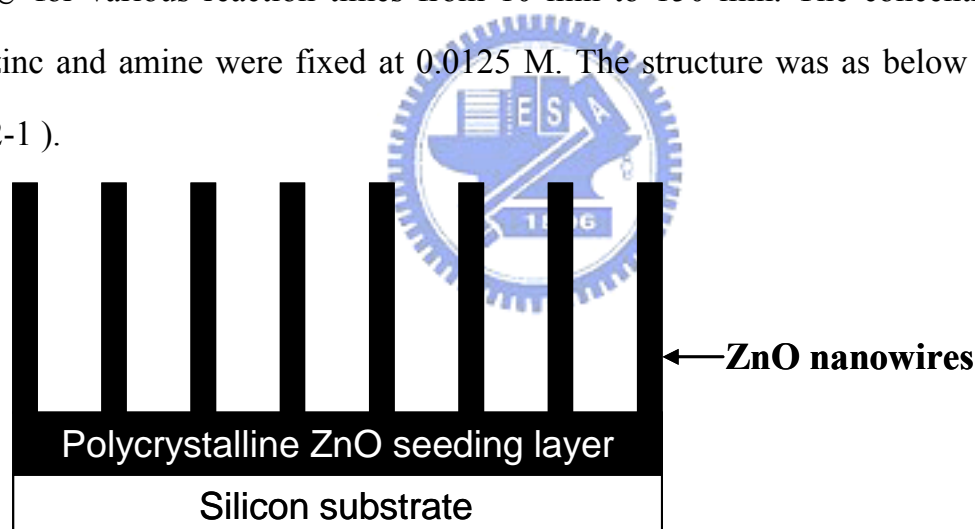


Figure 2-1. The structure of ZnO nanowires array.

2.2.4 Synthesized of ZnO/TiO₂ Core-shell Structures

The TiO₂ shell was deposited on ZnO nanowires by rf sputtering (13.56 MHz) under 10 mtorr Argon and Oxygen flow ratio 1:1 using home made TiO₂ target with vary sputtering power and time at 150°C . After TiO₂ was deposited, use the oven to anneal the ZnO/TiO₂ core-shell structure at 400°C and 500°C for 1 hour in the air. The structure was showed at Figure 2-2.

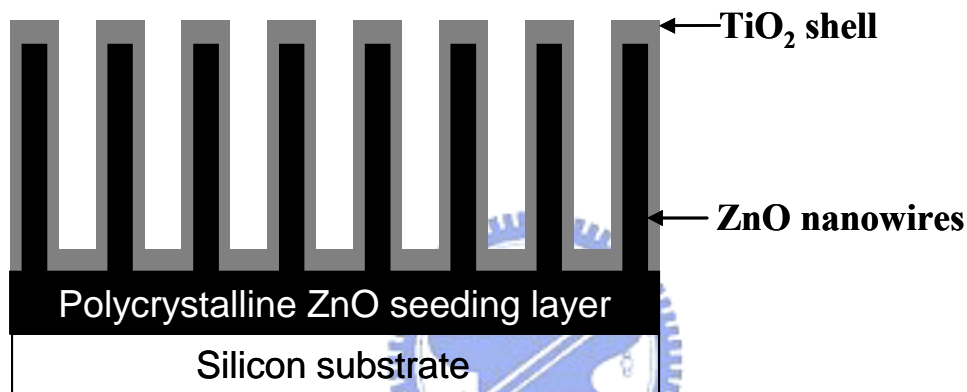


Figure 2-2. The structure ZnO/TiO₂ core-shell.

2.2.5 Synthesized TiO₂ Nanotubes

After the ZnO/TiO₂ core-shell structure nanowires were formed, the TiO₂ nanotubes was fabricated by wet-etching process. The ZnO nanowires were etched by the acetic acid (H₂O:CH₃COOH = 1000:1) for 30 min and 60 min. Beside, TiO₂ had very slow etch rate of acetic acid. So after the etch process the tubes- liked TiO₂ shell were still residual on the substructure. The structure was showed at Figure 2-3.

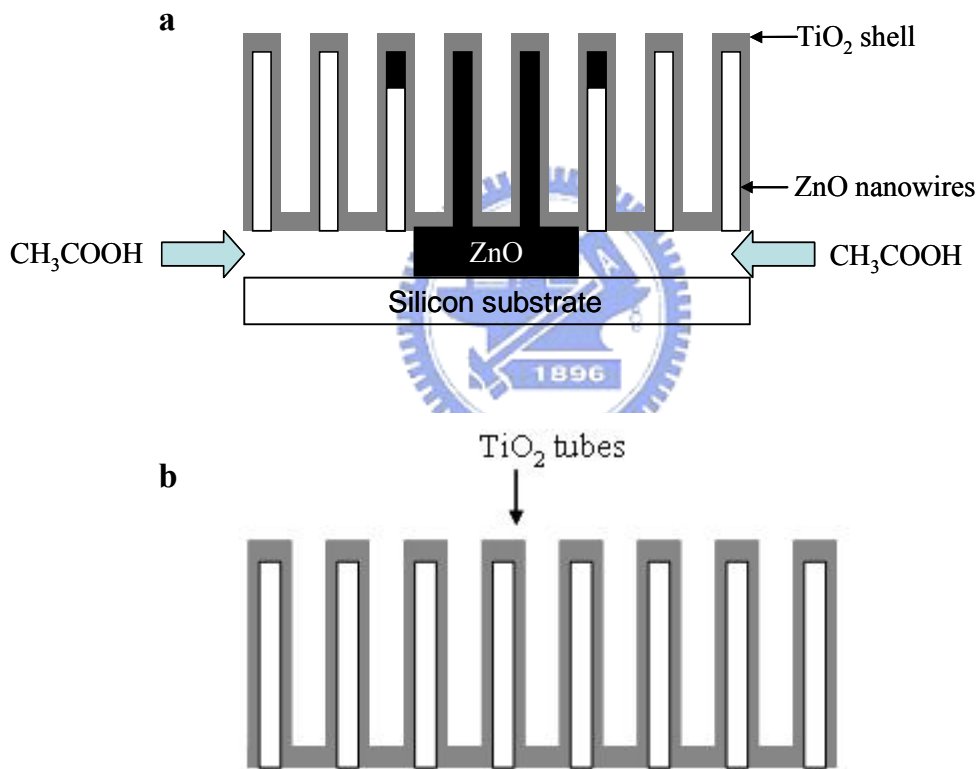


Figure 2-3. TiO₂ nanotubes was fabricated by wet-etching (a) 30 min (b) 60 min.

2.3 Measurement Equipment

The materials, electricity and electropotential analyses indicated that the several kinds characteristics of the ZnO NWs and ZnO/TiO₂ cores-shell structure. Through these analyses, the crystalline, lattice structure, defects of crystalline, chemical composition, morphology, field emission and photoluminescence could be understood easily.

2.3.1 Field Emission Scanning Electron Microscopy

(FE-SEM)

Scanning electron Microscopy (Hitachi S4700) was used to characterize the seed layer surface morphology, film thickness. Beside, it can also analyses the surface structure, morphology, diameter, length and density of ZnO/TiO₂ nanostructures. Hitachi S4700 with the resolution of 1.5 nm operated at 15 kV under 2×10^{-6} Torr. The cold field electron gun is used as the source of electron beam with the extraction voltage in the range from 0.5 kV to 30 kV.

2.3.2 High Resolution Transmission Electron

Microscopy (HR-TEM) and Dispersive X-Ray Energy

(EDX)

The structure and morphology analyses of ZnO nanowires, ZnO/TiO₂ core-shell and thickness of TiO₂ shell was measured by the high resolution transmission electron microscopy (JEM-2100F). The TEM is the equipment which produces the diffractive and scattering electrons by the interaction between substances and electrons. And by the selected area electron diffraction (SAED), it shows the crystalline structure of the ZnO nanowires and ZnO/TiO₂ core-shell. The HR-TEM shows that the lattice constants of the ZnO nanowires. In order to analyze the coverage of ZnO nanowires that were wrapped by the TiO₂, the EDX of the TEM is used. The fixed quantity analyses of the EDX is also used for the quantity of Zn, Ti and O.

The sample was put into the ultrasonic vibration. The rate of the vibration is about 14000 rpm. The vibration time is 3~5 minutes. And then the sample was scooped up from solution by a small copper grid a few mm in diameter.

2.3.3 X-Ray Diffraction (XRD)

The crystal structure of the ZnO nanowires and the ZnO/TiO₂ cores-hell structures were observed by the X-ray diffraction (Bede D1). X-ray diffraction (XRD) was the equipment most used for identifying the crystal structure. If the included angle θ (Bragg's angle) between the crystal plane and the incident light matched the Bragg's law ($n\lambda=2d\sin\theta$), the incident light was diffracted by

the crystal plane. By using Bragg's law for diffraction, the reflected x-rays from the respective atomic planes can be measured by the detector. In the Bragg's law ($n\lambda=2d\sin\theta$), $n\lambda$ is an integral number of wavelengths, and d is the distance between two successive crystal planes. On the basis of XRD data, the average grain size and orientations were determined. The average grain size of a specimen can be estimated from XRD peaks using Scherrer's formula by

$$D = \frac{0.9 \times \lambda}{B \times \cos(\theta)} \quad (2.1)$$

Where λ is the x-ray wavelength, 0.15405 nm, B means the full width at half maximum of the XRD peak, abbreviated as FWHM, and θ is taken as diffraction angle.

The X-ray diffraction measurement with Cu K α radiation ($\lambda=1.5418 \text{ \AA}$) was operated at 30KV and 20mA. In order to avoid the peak of silicon at about 70°, the angle 2 θ of the measurement was from 30° to 60°. The sweeping rate was 4° per minute.

2.3.4 Ultraviolet-Visible Spectrophotometers

In spectroscopy, the absorbance A is defined as

$$A_{\lambda} = \log_{10}(I_0/I)$$

Where I is the intensity of light at a specified wavelength λ that has passed through a sample (transmitted light intensity) and I_0 is the intensity of the light before it enters the sample or incident light intensity. Absorbance measurements are often carried out in analytical chemistry, since the absorbance of a sample is proportional to the thickness of the sample and the concentration of the absorbing species in the sample, in contrast to the transmittance I / I_0 of a sample, which varies exponentially with thickness and

concentration. See the Beer-Lambert law for a more complete discussion.

2.3.5 Cathodluminescence (CL)

The optical properties are measured by the Cathodluminescence spectrum (CL, JEOL JSM6500F, Japan) with an electron beam as an excitation source (15 KV) at room temperature. Cathodluminescence was a kind of nonsubversive optical measurement. By the analyses of Cathodluminescence (CL) spectrum, it can measure the band gap of solid materials and devices, and the defects and impurity of the materials. Different materials had different excitation source. When the light illuminates the sampl, the photon energy makes the electron of atom jump from ground state to excited state. Because the excited state was very unstable, the electron would subsequently jump to ground state. Between the transition of electron, the redundant energy would release in the form of heat energy or photon energy. The released energy was called the photoluminescence.

The Cathodluminescence spectrum is mainly used for measuring the optical spectrum. The excitation source is 15 KV. And the value of the photomultiplier tube (PMT) is -800V. The sweeping range is from 350nm to 700nm. The sweeping rate was 2nm per second.

2.3.6 Field Emission Detector

A Keithley 237 source-measure unit was used for measuring the current–voltage (I–V) and field emission characteristics. Field emission measurements were carried out in a vacuum chamber with a pressure of 5×10^{-6} Torr at room temperature. A copper electrode probe adopted as an anode with an area of 7.1×10^{-3} cm² was placed at different distances from tips of nanostructures. The measurement equipment was illustrated in Figure 2-4.

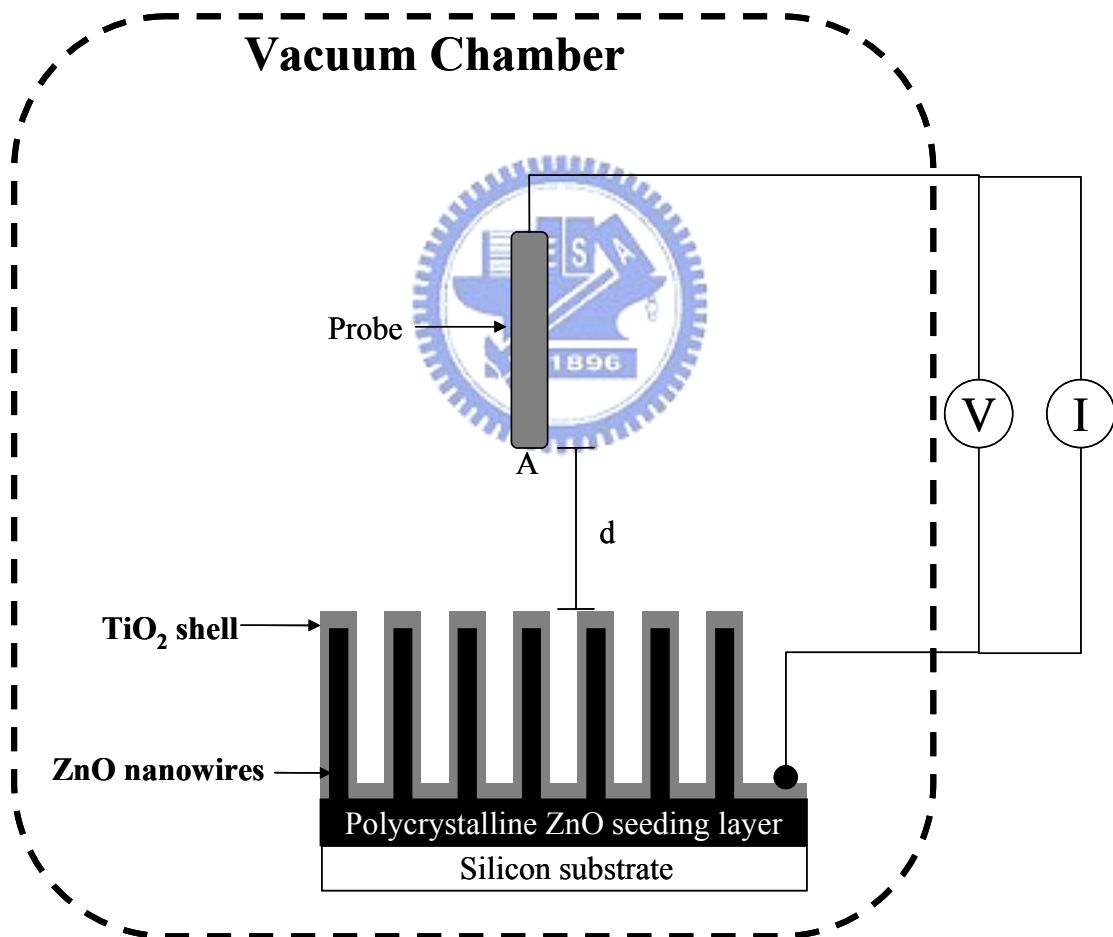


Figure 2-4. Schematic diagram of a high-vacuum chamber system for field emission property measurement.

Chapter 3 Results and Discussion

3.1 ZnO Seeding Layer

In order to fabricate the well-aligned ZnO nanowires on Si substrate, we deposited a ZnO thin film on the substrate as a seeding layer. Because of there is a high lattice mismatch between Si and ZnO. The high lattice mismatch leads to grow well-aligned ZnO nanowires difficulty. After depositing the ZnO (002) thin film on the Si substrate, the lattice mismatch became smaller. Beside, ZnO (002) thin film can help ZnO growth along (002) to form well-aligned ZnO nanowires.

The thickness and the qualities of the ZnO seeding layer must be suitable. First, it must have had a dominant orientation along (002). Second, the thickness of ZnO seeding layer must be suitable. If it was too thin, the lattice mismatch was still high. It will be hard to form ZnO nanowires and that is easy to form another type ZnO nanostructures such as tetrapod ZnO nanorods and ZnO nanoflowers as shown in the Figure 3-1. If ZnO seeding layer is too thick, the adsorption and resistance of the film will be higher. So, if ZnO seeding layer is too thick, this process is hard to be used in the solar cells or field emission device.

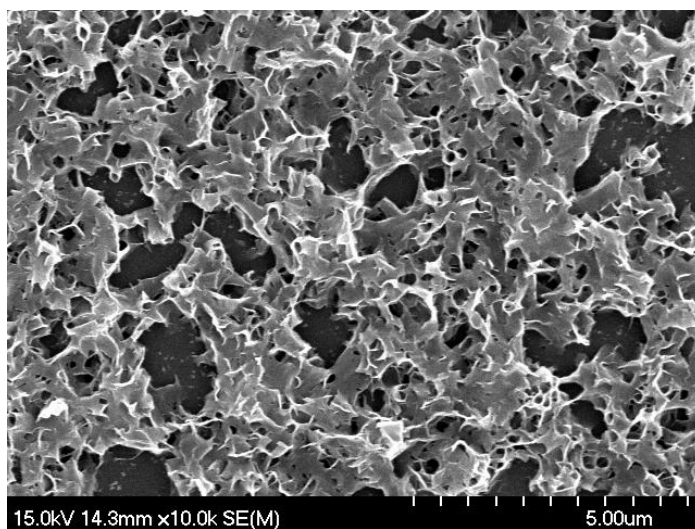


Figure 3-1. SEM image of ZnO nanoflowers.

3.1.1 The Field Emission Scanning Electron Microscopy

Analyses

The epitaxial ZnO seeding layer was deposited by the RF-sputtering (30W at 1×10^{-2} torr for 30 min at room temperature under Ar and O₂ flowing rate 3:1). The thickness of the epitaxial ZnO seeding layer was about 60 nm. Figure 3-2 shows the top-view and cross-section SEM micrographs of the ZnO seeding layer grown on the Si substrate after annealing at 750°C 3 hours under a keeping O₂ flow rate of 30 sccm.

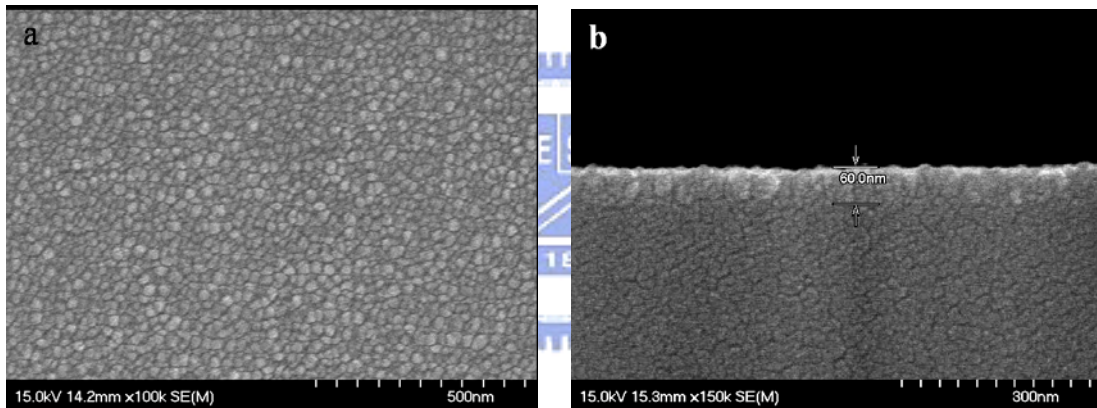


Figure 3-2. The SEM image of ZnO seeding layer on the Si substrate. (a) Top view (b) cross section.

3.1.2 The X-Ray Diffraction Analyses

Figure 3-3 shows the XRD patterns of ZnO seeding layer on Si substrate as deposition and after thermal annealing at 750°C 3 hours under a keeping O₂ flow rate of 30 sccm. It implied that the ZnO thin film has preferred orientation along (002) after annealing.

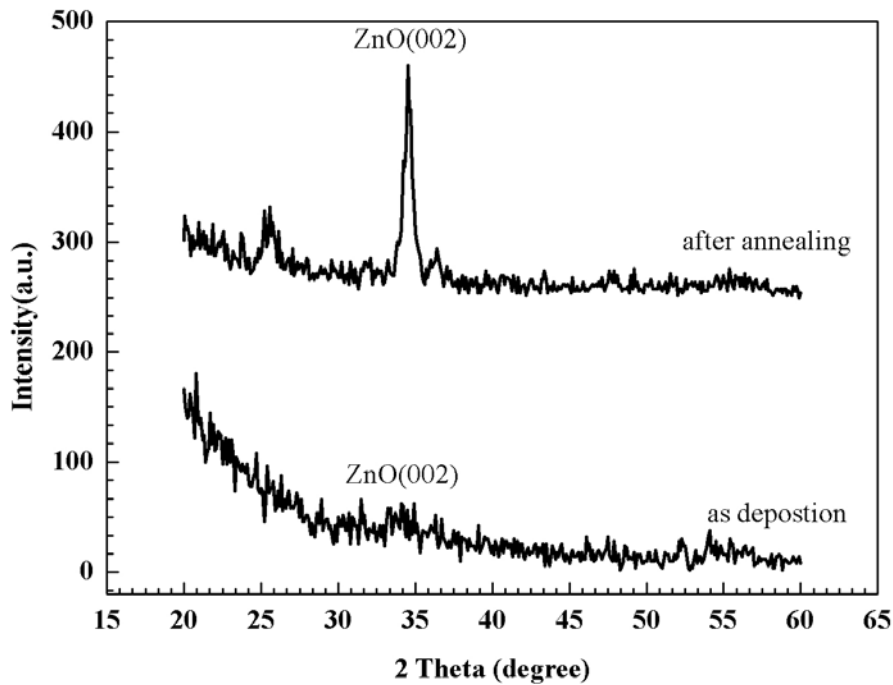


Figure 3-3. XRD patterns of ZnO seeding layer on Si substrate as deposition and after thermal annealing at 750°C 3 hours.

3.1.3 Ultraviolet-Visible Spectrophotometers Analyses

Figure 3-4 show the transmittance spectra of ZnO seeding layer. It shows a low transmittance region at 250 nm-370 nm. It is because the energy band gap of ZnO is 3.37 eV. And at visible region, it shows a very high transmittance (>90 %).

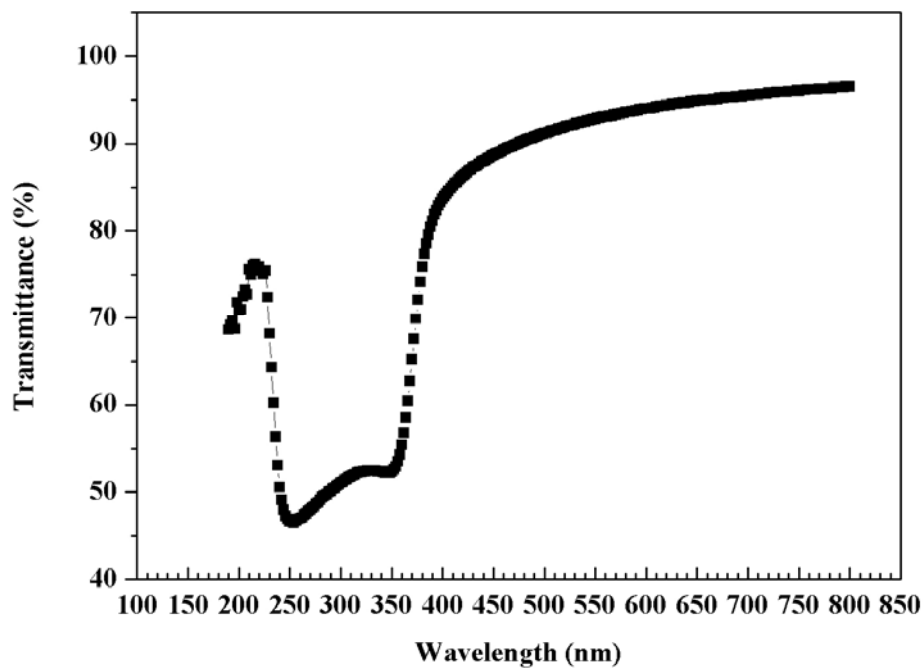


Figure 3-4. The transmittance spectra of ZnO seeding layer.

3.2 ZnO Nanowires

The ZnO nanowires were synthesized by the hydrothermal method. The hydrothermal process has several advantages over other growth processes such as catalyst-free growth, low cost, large area uniform production, environmental friendliness, and low reaction temperature to integrate into the microelectronics. The source of the hydrothermal method was zinc nitrate hexahydrate ($\text{Zn}(\text{NO}_3)_2 \cdot 6\text{H}_2\text{O}$, (99.9%)) and hexamethylenetetramine (HMTA ; $\text{C}_6\text{H}_{12}\text{N}_4$, (99.9%)). The chemical solution was mixed with the ratio of 1:1. The Figure 3-5 was the pourbaix diagram for zinc. From the pourbaix diagram, if we want to form ZnO the pH value of the solution must control between 6 and 14. If the pH value of the solution was not between 6 and 14, there were many other compounds produced. The compounds included $\text{Zn}^{2+}_{(\text{aq})}$, $\text{Zn}_{(\text{s})}$ and $\text{Zn}(\text{OH})_4^{2-}_{(\text{aq})}$. The pH value of the concentration from 0.01M to 0.5M before growing is between 6 and 8 testing form the litmus paper. So in the experiment, it can grow ZnO nanowires. The pH value of the concentration after growing is lower than that before growing.

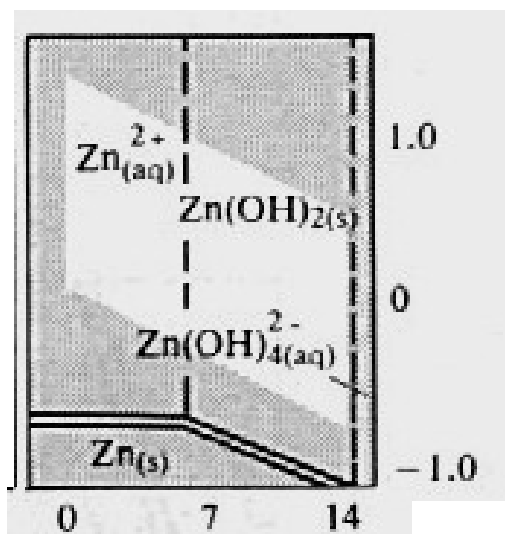


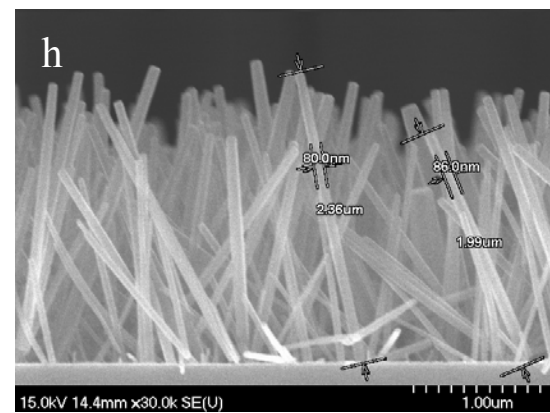
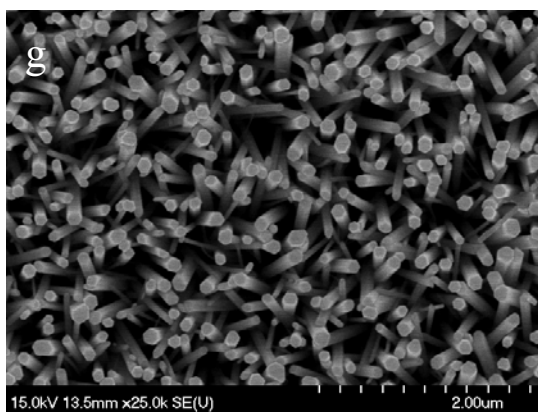
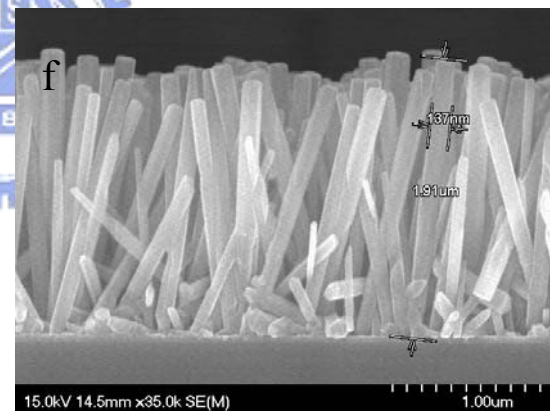
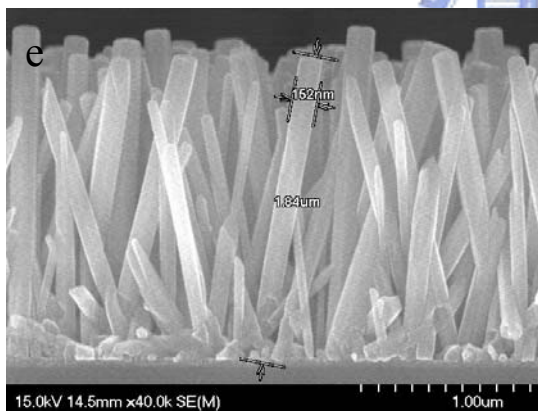
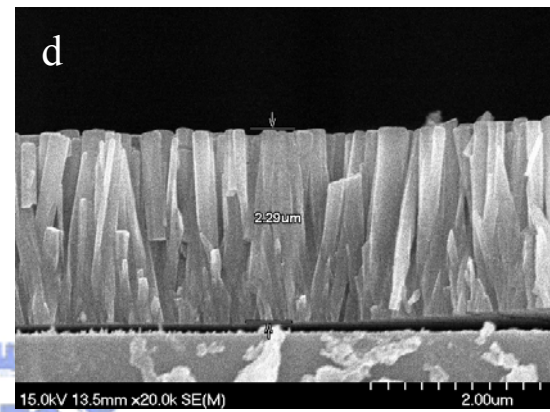
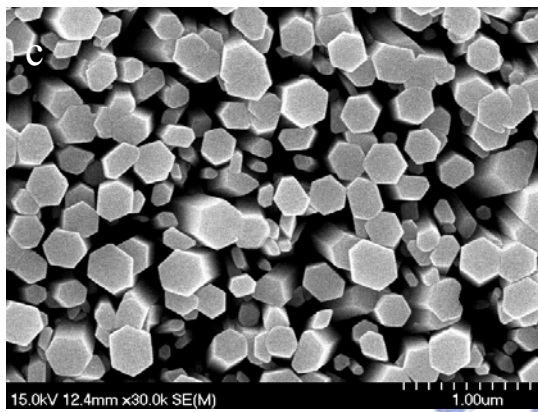
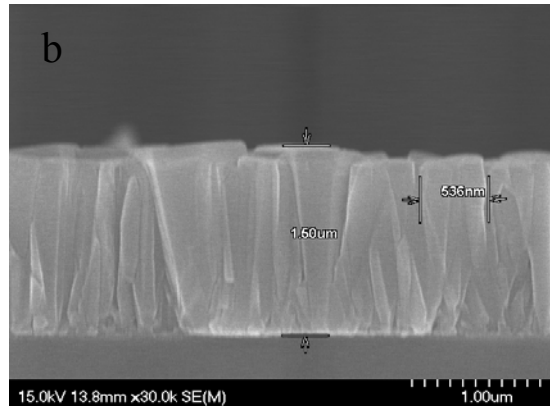
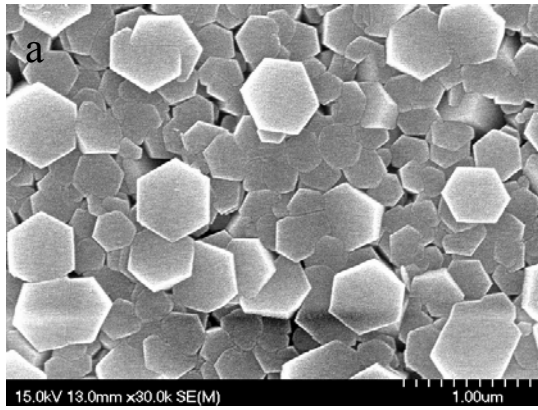
Figure 3-5. The pourbaix diagram of the $\text{Zn}(\text{OH})_2$.

3.2.1 Characterization of ZnO Nanowires

The chemical solution concentration

The chemical solution concentration is a key factor of growing ZnO nanowires by the hydrothermal method. We changed the concentration from 0.5 M to 0.01M under the same growth time (3 hours) and same temperature (95°C). As raising the concentration of the chemical solution the ZnO nanowires become denser. When the concentration of the chemical solution was 0.5 M, the density of the ZnO nanowires was very high and it became a ZnO film. Beside, as decreasing the concentration of the chemical solution the diameter of the ZnO nanowires became smaller. The surface morphologies of the ZnO nanowires in different concentration of the chemical solution under the same growth time were shown in Figure 3-6. From the Figure 3-7, it is easy to observe that the aspect ratios of ZnO nanowires with different concentration of the chemical solution are different. Generally, the concentration of the chemical solution are higher the aspect ratios of ZnO nanowire are smaller. But the aspect ratio of ZnO nanowires grew at 0.01 M is lower than grew at 0.0125 M. It may be because that the source of 0.01 M is not enough for ZnO nanowires growing longer. So the aspect ratio is lower.

In order to fabricate the ZnO nanowires which have the better field emission characteristic or high surface area, we choose the concentration (0.0125 M) with highest aspect ratio of ZnO nanowires.



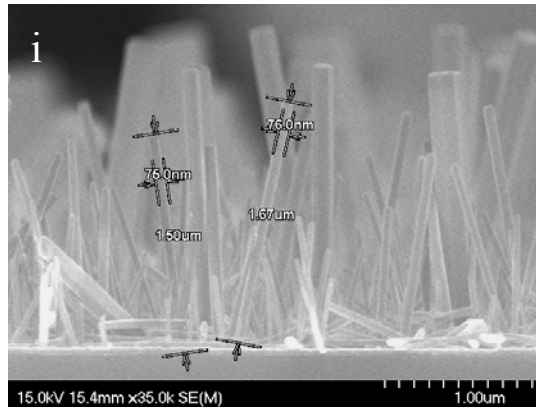


Figure 3-6. The SEM image ZnO nanowires grew in (a) 0.5 M (top view) (b) 0.5 M (cross section) (c) 0.1 M (top view) (d) 0.1 M (cross section) (e) 0.05 M (cross section) (f) 0.025 M (cross section) (g) 0.0125 M (top view) (h) 0.0125 M (cross section) (i) 0.01 M (cross section).

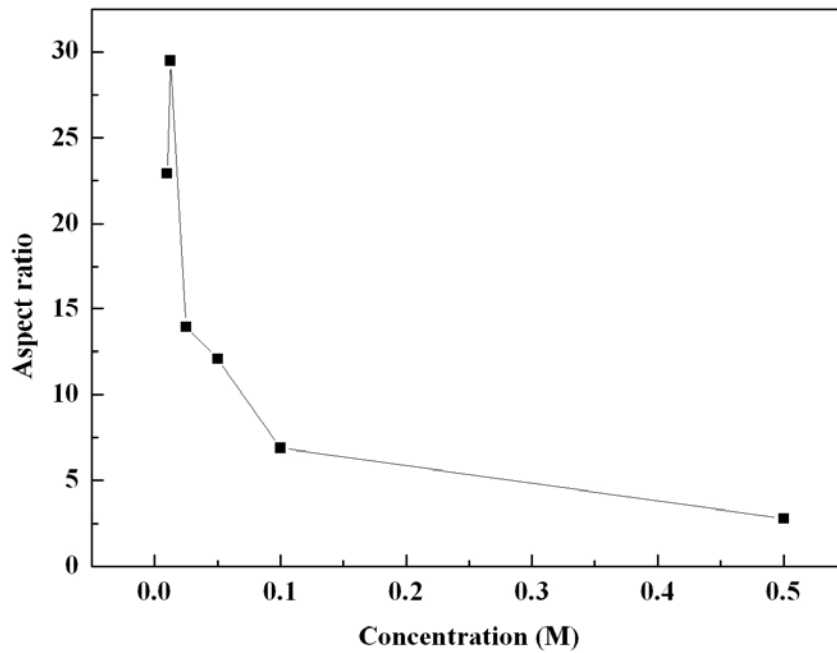


Figure 3-7. Aspect ratio of ZnO nanowires as a function of concentration.

The growth time

The growth time of ZnO nanowires is another important parameter of hydrothermal method. In the experiment, we controlled the growth time from 30 min to 3 hours under the same concentration (0.0125M) of the chemical solution and keep in the same temperature (95°C). The morphologies of the ZnO nanowires with different growth time show in Figure 3-8. If the growth time is below 60min, there are no nanowires on the substrate. The dependence of the length of nanowires on growth time is illustrated in Figure 3-9. Observe from the Figure 3-9, there are two distinct growth kinetics: a very fast step, which takes from 60 min to 105 min with a growth rate of 43.99 nm/min and a relatively slow step with a growth rate of 2.70 nm/min, the fast step is about 16 times of the rate in the slow step.

Figure 3-10 show the XRD patterns of ZnO nanowires growing for 70 min and 120min. It implies that ZnO nanowires with growing 120 min had stronger peak of (002).

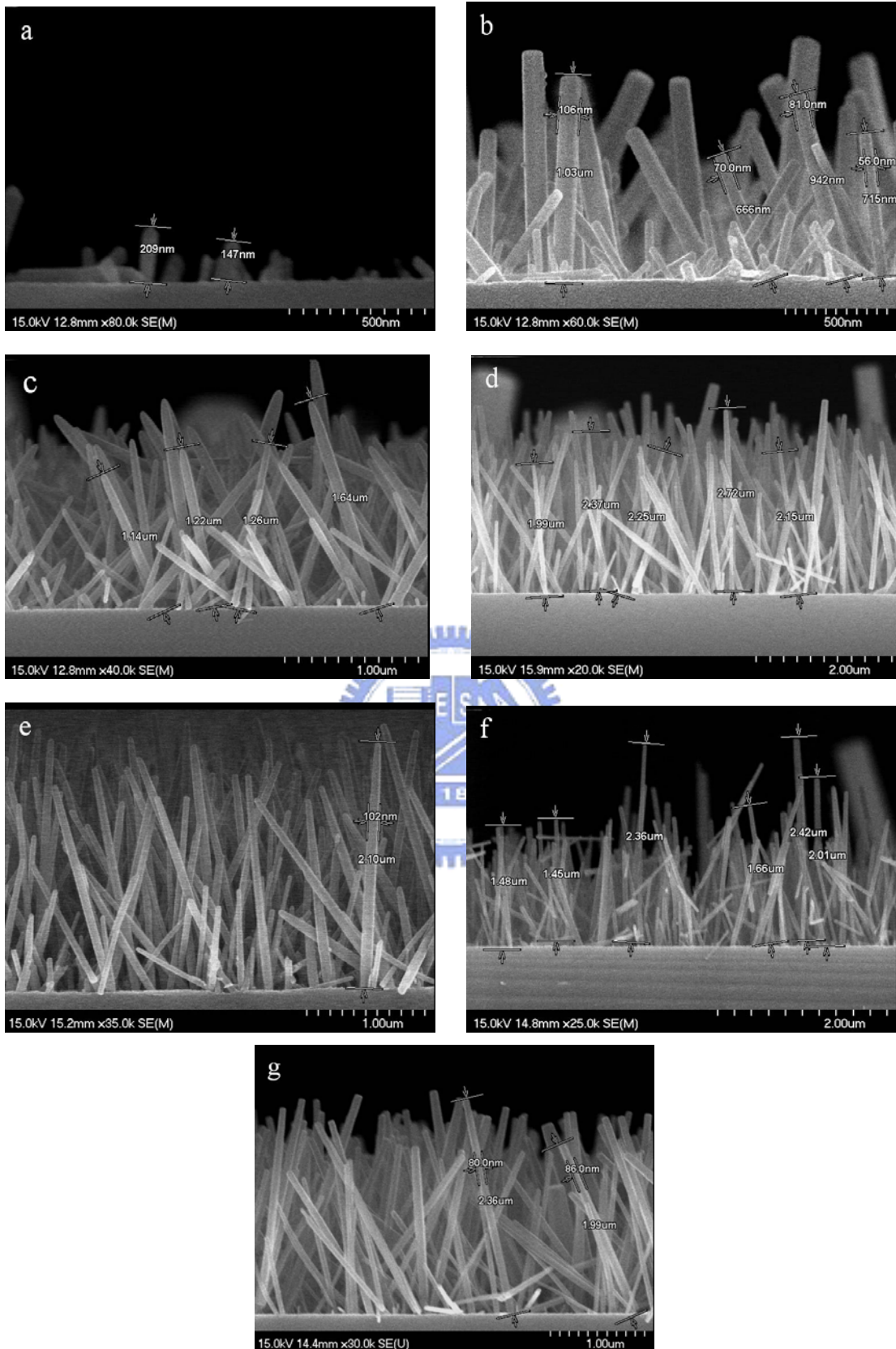


Figure 3-8. (a) Cross-section FE-SEM micrographs of ZnO nanowires at 0.0125 M with growing 60min (b) 75 min (c) 90 min (d) 105 min (e)120 min (f) 150 min (g) 180 min.

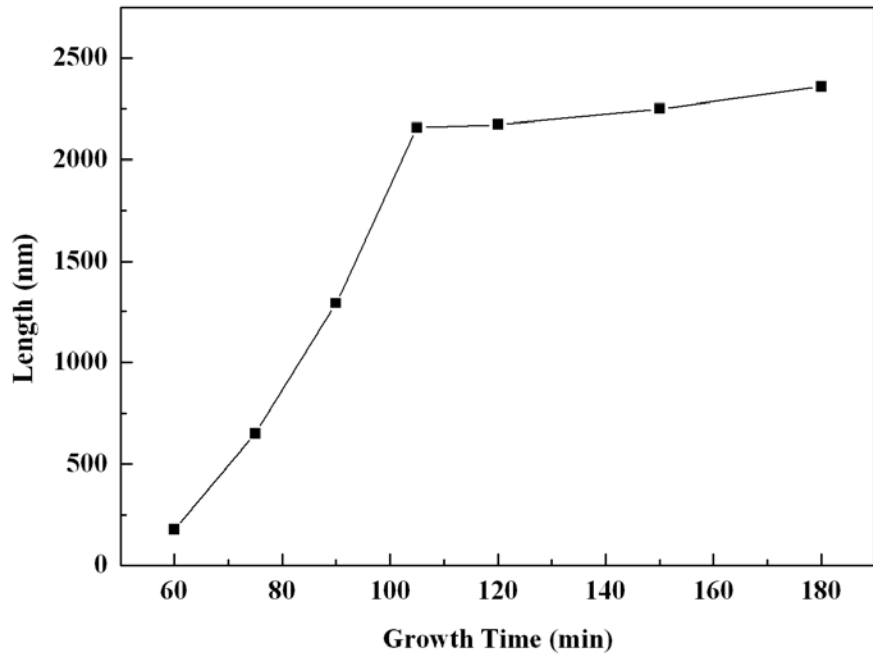


Figure 3-9. Average length of ZnO nanowires as a function of growth time.

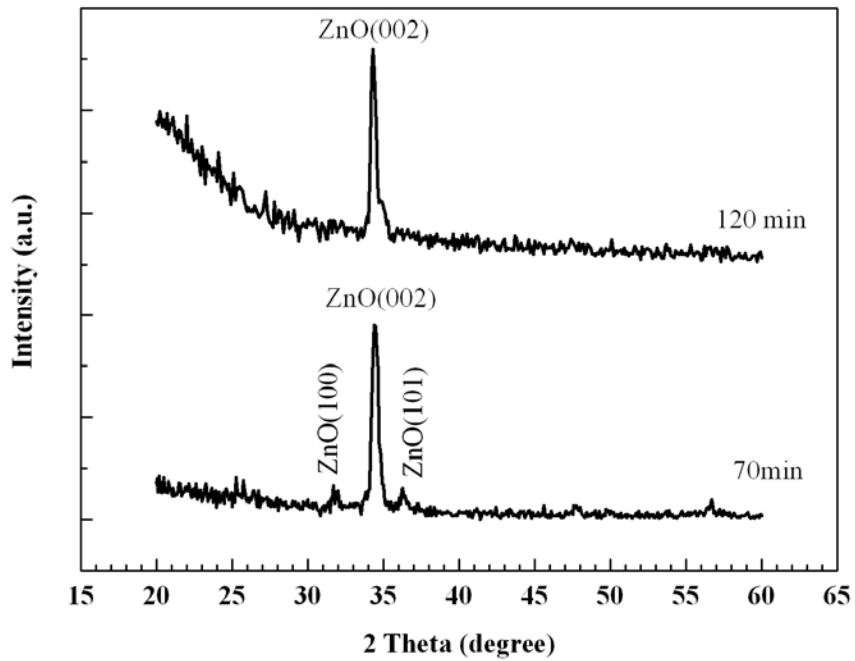


Figure 3-10. The X-ray diffraction pattern of ZnO nanowires grown on Si wafer with different growth time (a) 70 min (b) 120 min.

3.2.2 The Optical Properties

ZnO is a well-known semiconductor for its wide band gap and high exciton binding energy at room temperature. When the scale of system is under 100 nm, the new optical phenomenon may occur. So, it is important to understand the optical properties of the ZnO nanowires. Figure 3-11 shows the cathodluminescence (CL) spectra of ZnO nanowires with different growing time. The peaks of UV were both at about 374 nm (3.321eV). It is different with the ZnO band gap was 3.37 eV. It is because that the 3.321 eV was the band gap between the valence band and the excited state. The main peak of the visible light region is at about 575 nm (2.16 eV). By the figure 1-6, the deep-level emission is caused by the energy interval between the oxygen vacancies V_O level 766.9 nm (1.62 eV), single ionized oxygen vacancies V_O^* level 540.24 nm (2.3eV) and oxygen interstitial O_i level 544.9 nm (2.28 eV). The peak at 620 nm is the error of detector. The cathodluminescence (CL) mainly measured the UV signal from the valence band to the excited state.

Generally, there are two types of defects in the ZnO, one is the radiative defects and the other is nonradiative defects. The radiative defects were V_O , V_O^* , Zn_i , V_{Zn} , O_i and O_{Zn} . The nonradiative defects were the surface defects, the lattice defects and etc.

When the ZnO nanowires formed by the hydrothermal method, the chemical component of the ZnO nanowires was nonstoichiometric, and usually consisted of excess Zn atoms and oxygen vacancies. After the ZnO nanowires formed, the surface of the ZnO nanowires was very unstable. It is easy to adsorb the steam and the impurities in the air to become the stable state on the surface of the ZnO nanowires. In other words, the steam and the impurities

formed the surface defects on the ZnO nanowires. These defects will make the UV intensity lower and luminescence higher.

From figure Figure 3-11, it can fine that the ZnO nanowires for 120 min had stronger UV peak and lower visible light region then the ZnO nanowire for 70 min. It means that the defects in the ZnO nanowires for 70 min are more than the defects in the ZnO nanowires for 120 min.

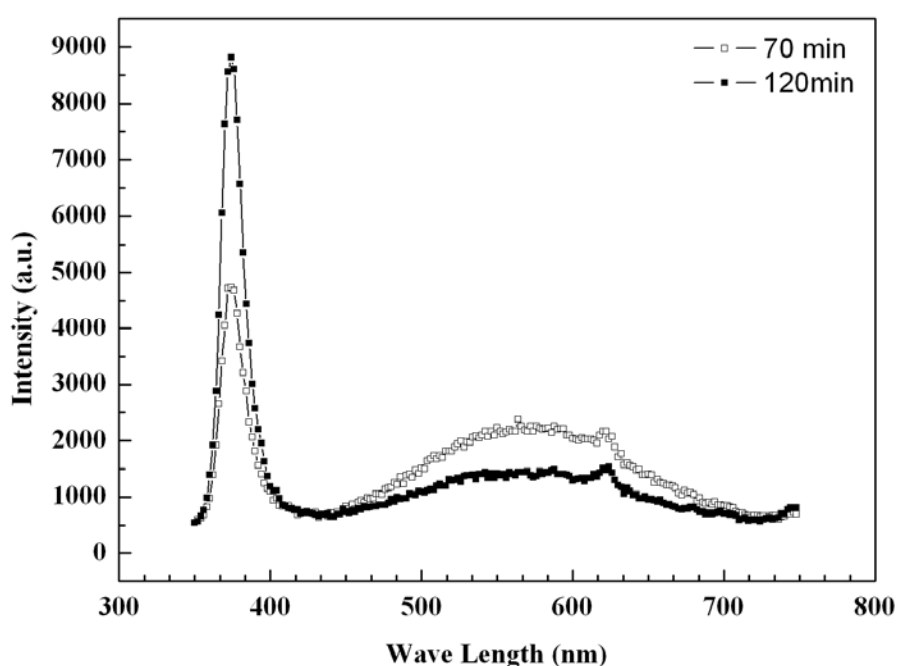


Figure 3-11. The CL spectra of ZnO nanowires for 70min and 120 min.

In order to decrease the defects of the ZnO nanowires, we put ZnO nanowires in the oven for thermal process. Figure 3-12 shows the cathodluminescence (CL) spectra of the ZnO nanowire annealing at 400°C 1 hour under the air. The visible region decreased after the thermal treatment clearly. It means that the defects in the ZnO nanowires which were formed by hydrothermal method were restored after thermal treatment.

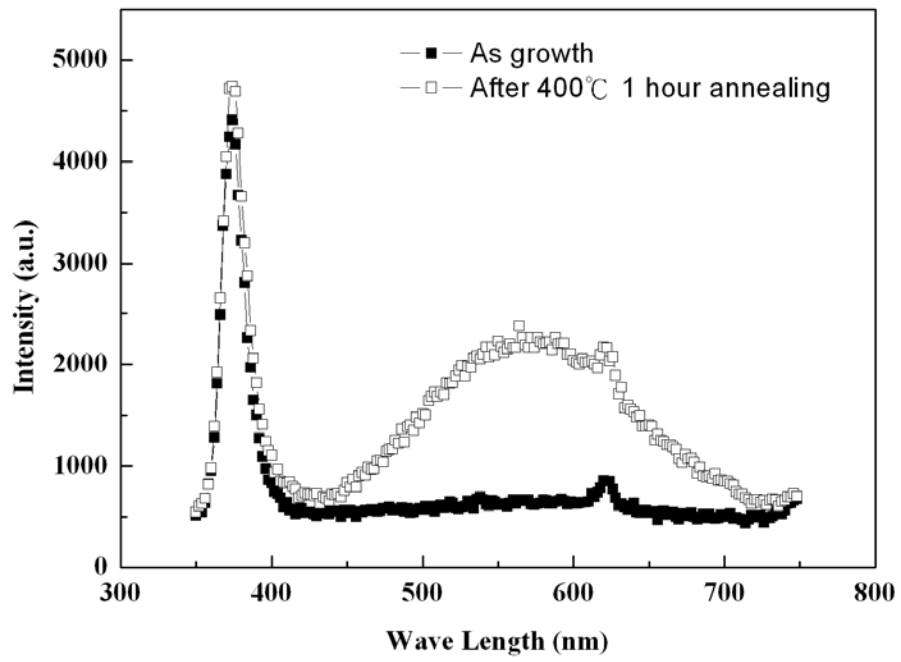


Figure 3-12. The CL spectra of ZnO nanowires as growth and after annealing.



3.2.3 The Field Emission Properties

First, we show the Fowler-Nordhiem (F-N) function, which details were introduced at section 1-5.

$$J = \frac{A\beta^2 E^2}{\Phi} \exp\left[-\frac{B\Phi^{\frac{3}{2}}}{\beta E}\right] \quad [3.1]$$

$$A = 1.56 \times 10^{-10} (AV^{-2}eV) \quad [3.2]$$

$$B = 6.83 \times 10^3 (eV^{-\frac{3}{2}}V/\mu m) \quad [3.3]$$

$$\ln\left(\frac{J}{E^2}\right) = -\frac{B\Phi^{\frac{3}{2}}}{\beta} \frac{1}{E} + \ln\left(\frac{A\beta^2}{\Phi}\right) \quad [3.4]$$

$$m = -\frac{B\Phi^{\frac{3}{2}}}{\beta} \quad [3.5]$$

The J-E curves of ZnO nanowires on the Si substrate with different growth time are show in Figure 3-13. As show in figure, the ZnO nanowires with growth time 120 min had the better field emission property. The turn on field (E_{on}) defined as the electric field under the current density at $1.0 \mu A/cm^2$ and the threshold filed (V_{th}) defined as the electric field under the current density at $1.0 \mu A/cm^2$. The turn on voltage (V_{on}) of ZnO nanowires with growth time 70 min, 90 min, 105 min, 120 min are $5 V/\mu m$, $3.28 V/\mu m$, $2.95 V/\mu m$, $2.7 V/\mu m$, respectively. The work function of ZnO is $5.37 eV^{39}$. The field enhance factor β can be calculated from the slop of the F-N plots (equation 3.5). The corresponding F-N plots of ZnO nanowires on the Si substrate with different growth time are showed in Figure 3-14. The field enhance factor β of Zno nanowies with different growth time 70 min, 90 min,

105 min, 120 min are 1039.8, 1464.25, 2082.1, 2475.8, respectively. The detail data of field emission property are showed in

Table 3-1.

It is well know that the β value depends on the geometry, structure, tip size and the number density of the emitters on the substrate. The ZnO nanowire with time 120 min had largest β . This phenomenon can be explained that a longer length of ZnO nanowires had better aspect ratio. It means that the point discharge effect is stronger, and consequently it provide the lowest turn on filed.

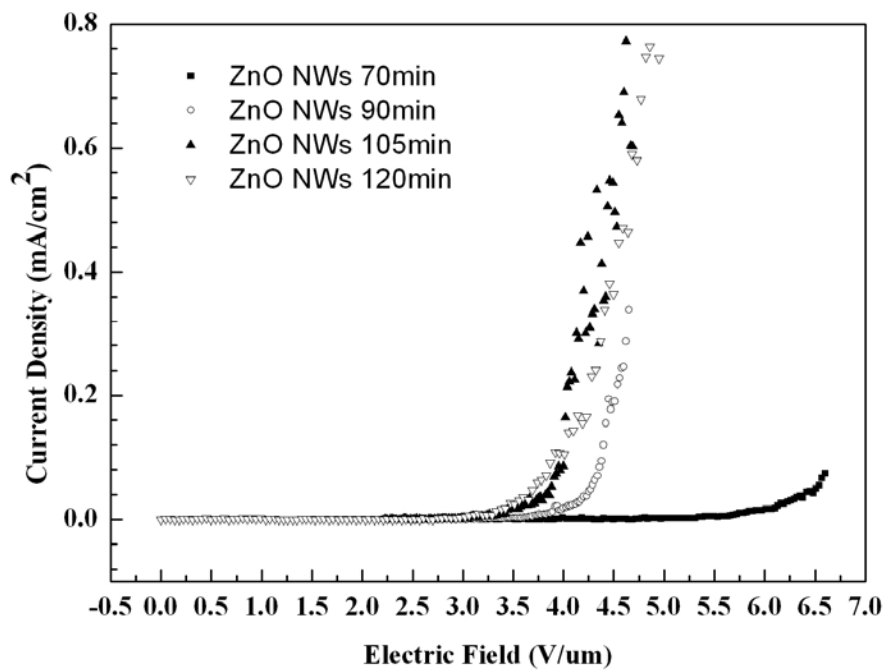


Figure 3-13. Field emission current-voltage curves of ZnO nanowires with different growth time.

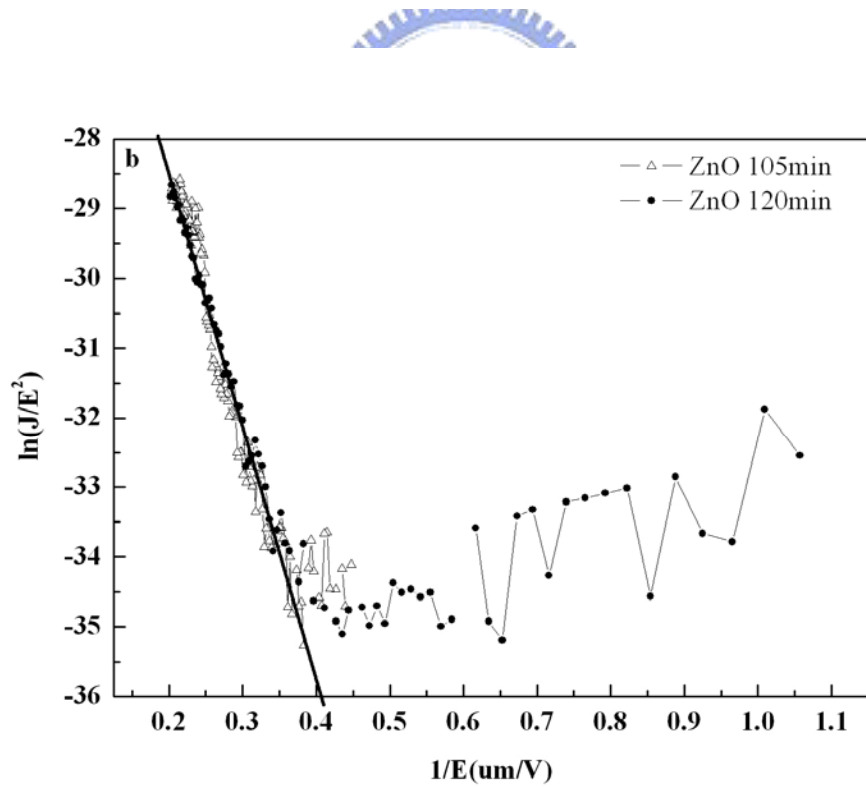
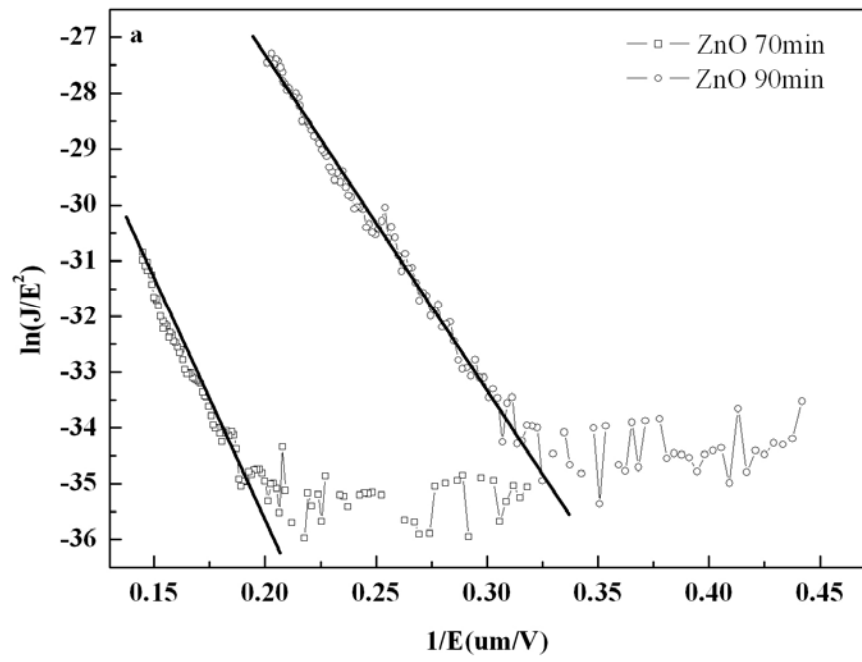


Figure 3-14. The Fowler-Nordhiem (F-N) plots of ZnO nanowires with different growth time

	70 min	90min	105 min	120 min
Electrode Area	0.00709(cm ²)	0.00709(cm ²)	0.00709(cm ²)	0.00709(cm ²)
Work Function	5.37 eV (ZnO)	5.37 eV (ZnO)	5.37 eV (ZnO)	5.37 eV (ZnO)
Eon	5 (V/μm)	3.28 (V/μm)	2.95 (V/μm)	2.75 (V/μm)
Eth	x	4.64 (V/μm)	x	x
Slope of F-N plots	82.1	58.3	41	34.47
β	1039.8	1464.25	2082.1	2475.8
Average Length	649.25 (nm)	1291.3 (nm)	2157.5 (nm)	2173.3 (nm)

Table 3-1. The detail data of field emission property of ZnO nanowires with different growth time.



3.3 ZnO/TiO₂ Core-shell Nanowires

In order to fabricate the ZnO/TiO₂ core-shell nanowires, the ZnO nanowires must grow on the Si substrate by hydrothermal method first. The ZnO nanowires array had been fabricated, as show in the Figure 3-9.

Now we are focused on the TiO₂ shell deposition process. The TiO₂ shell was deposited on ZnO nanowires by RF sputtering (13.56 MHz) under 5 mtorr Argon and Oxygen flow ratio 1:1 using TiO₂ target at different sputtering power, time and deposition temperature.

3.3.1 The Field Emission Scanning Electron Microscopy

Analyses

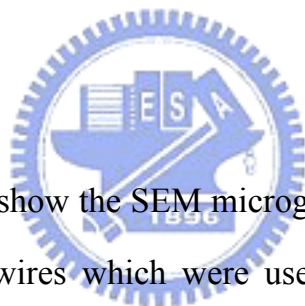


Figure 3-15 & Figure 3-16 show the SEM micrographs of ZnO/TiO₂ core-shell nanowires. The ZnO nanowires which were used to fabricate the core-shell nanowires are 0.0125 M at 70 min and 120 min. Observe from Figure 3-15, it is easy to find that those core-shell nanowires are different to others. It is because that the TiO₂ deposited at room temperature is not uniform. And others are deposition at 150°C. In the other words, it means that higher deposition temperature can get uniform TiO₂ thin film on the ZnO nanowires. It may be because that increase the deposition temperature can increase the mean free path of TiO₂ in the chamber and deposited the uniform TiO₂ thin film.

Figure 3-16 show the SEM images of ZnO/TiO₂ nanowires with different deposition power and deposition time of sputtering TiO₂. It is hard to find the difference between ZnO nanowires and ZnO/TiO₂ core-shell nanowires. It is because that TiO₂ on the ZnO nanowires is very thin and uniform. Another

reason is that the resolution of SEM is not enough. In the next section, we will discuss the ZnO/TiO₂ nanowires by HR-TEM analyses.

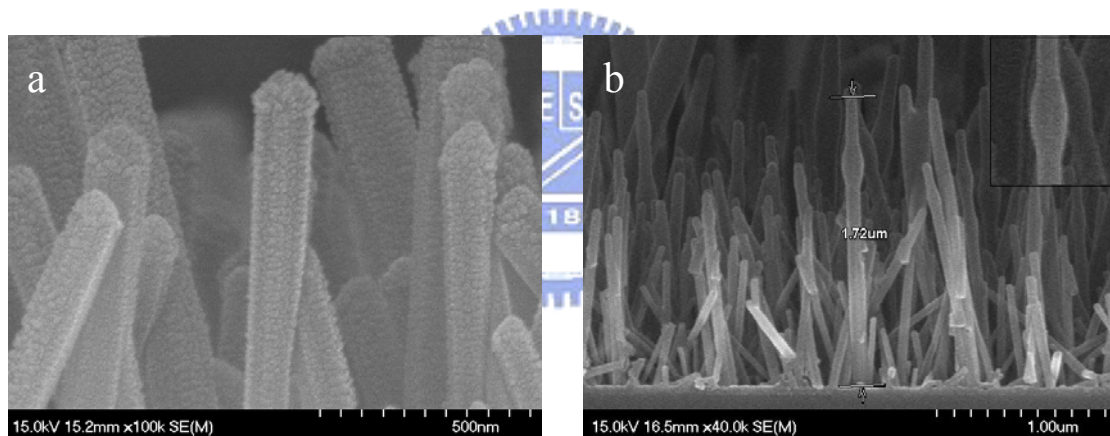
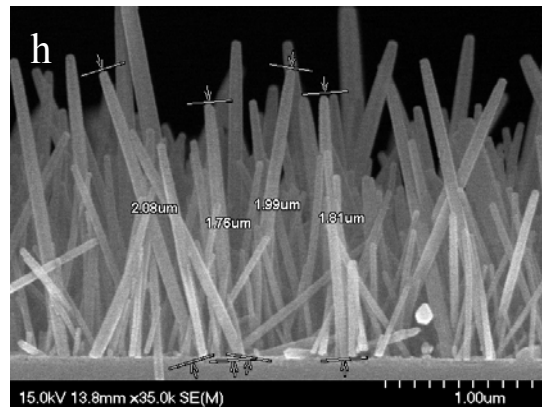
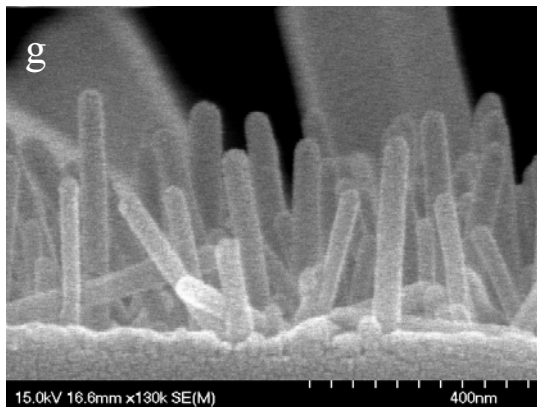
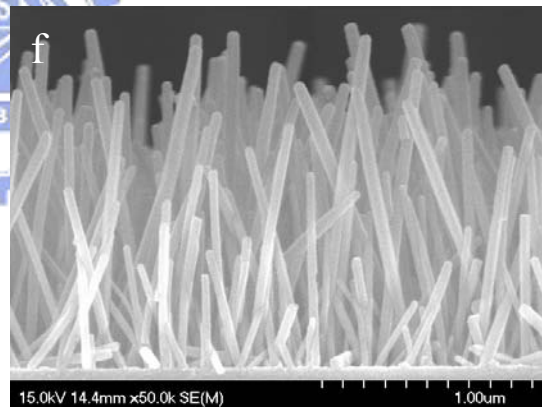
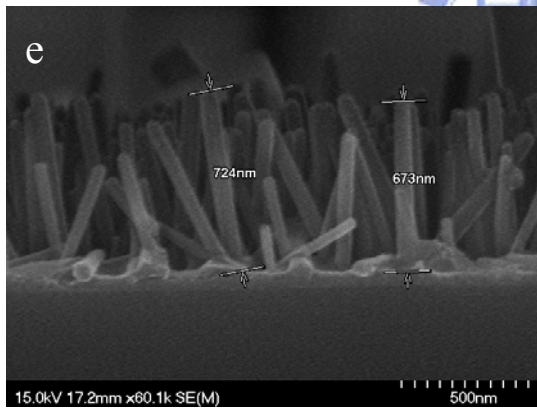
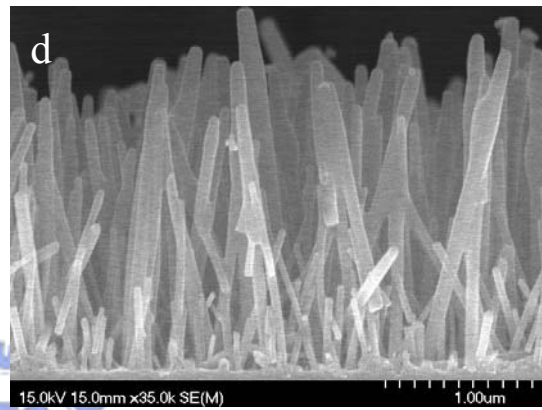
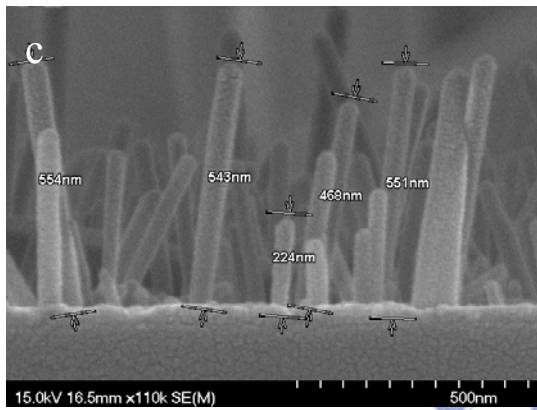
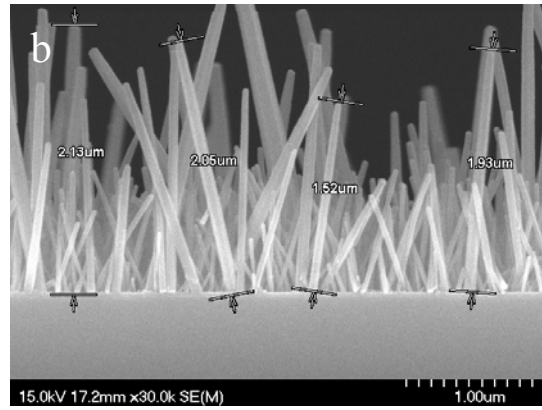
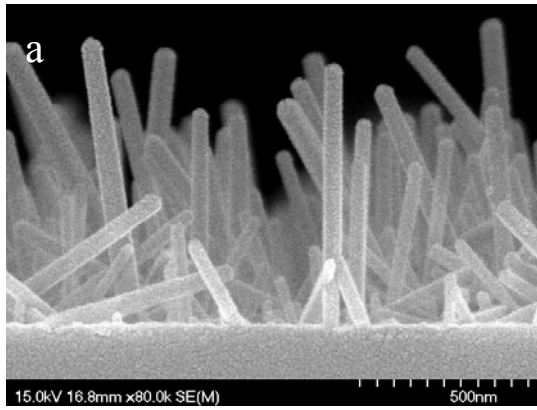


Figure 3-15. SEM images of ZnO/TiO₂ core-shell nanowires deposited at room temperature.



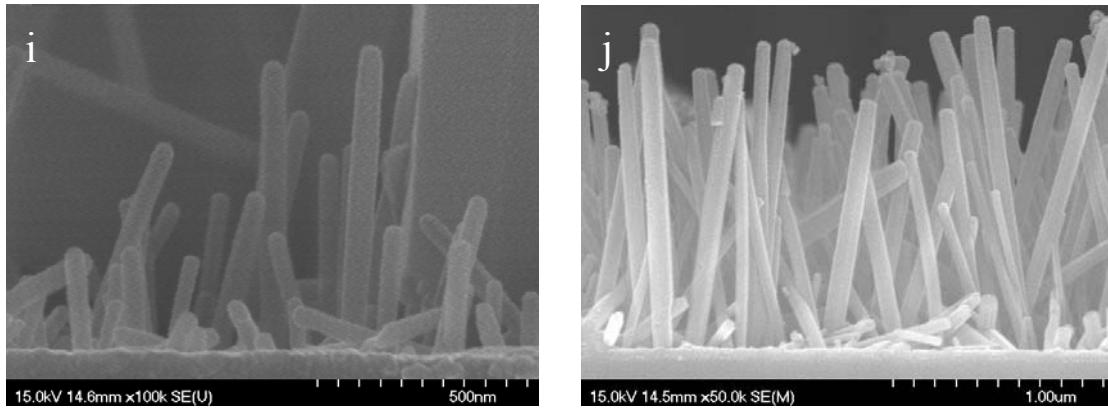


Figure 3-16. SEM images of ZnO/TiO₂ core-shell nanowires with different sputter parameters.

- (a) ZnO nanowires grew 70 min and deposited TiO₂ for 30w 30min at 150°C
- (b) ZnO nanowires grew 120 min and deposited TiO₂ for 30w 30min at 150°C
- (c) ZnO nanowires grew 70 min and deposited TiO₂ for 60w 30min at 150°C
- (d) ZnO nanowires grew 120 min and deposited TiO₂ for 60w 30min at 150°C
- (e) ZnO nanowires grew 70 min and deposited TiO₂ for 90w 30min at 150°C
- (f) ZnO nanowires grew 120 min and deposited TiO₂ for 90w 30min at 150°C
- (g) ZnO nanowires grew 70 min and deposited TiO₂ for 60w 60min at 150°C
- (h) ZnO nanowires grew 120 min and deposited TiO₂ for 60w 60min at 150°C
- (i) ZnO nanowires grew 70 min and deposited TiO₂ for 90w 90min at 150°C
- (j) ZnO nanowires grew 120 min and deposited TiO₂ for 90w 90min at 150°C

3.3.2 The High Resolution Transmission Electron

Microscopy and Dispersive X-Ray Energy Analyses

HR-TEM images and correspond selected area electron diffraction (SAED) pattern are showed in Figure 3-17, which illustrates the appearance and crystal structure of the ZnO/TiO₂ core-shell nanowires. The ZnO nanowires grew for 70 min, and the TiO₂ shell is deposition by sputter system with 90 W 90 min at 150°C. From Figure 3-17a, the structure had arc like tip. It is because TiO₂ is easier deposited on the tip center of ZnO nanowires. The diameter and length of this structure are 671.5 nm and 54.23 nm, respectively. Figure 3-17b-d are the images of region A, B and C, respectively. Form the Figure 3-17b, there is a TiO₂ shell with 4.15 nm, 6.93 nm and 11.26 nm at right, left and top clearly. From the Figure 3-17c, there is a TiO₂ shell with 4.14 nm and 8.55 nm at right and left side. Form the Figure 3-17d, there is a TiO₂ shell with 4.32 nm at left side. The thickness of TiO₂ is not the same. It may be because the ZnO nanowire did not stand on the substrate straightly. And it is found that ZnO nanowires grow along the [002] direction. The distance between parallel [002] is 2.6Å. The corresponding selected area electron diffraction (SAED) pattern of the core-shell structure is shown in Figure 3-17f. It shows that the ZnO nanowire is a single-crystalline structure with coating an amorphous TiO₂ film. Table 3-2 shows the atomic percentage of ZnO/TiO₂ core-shell structure analyses by EDX. It means that the tip of ZnO nanowire have a lot of TiO₂. It is because that it is easier to deposit TiO₂ on top plane than other plane by RF-sputtering system.

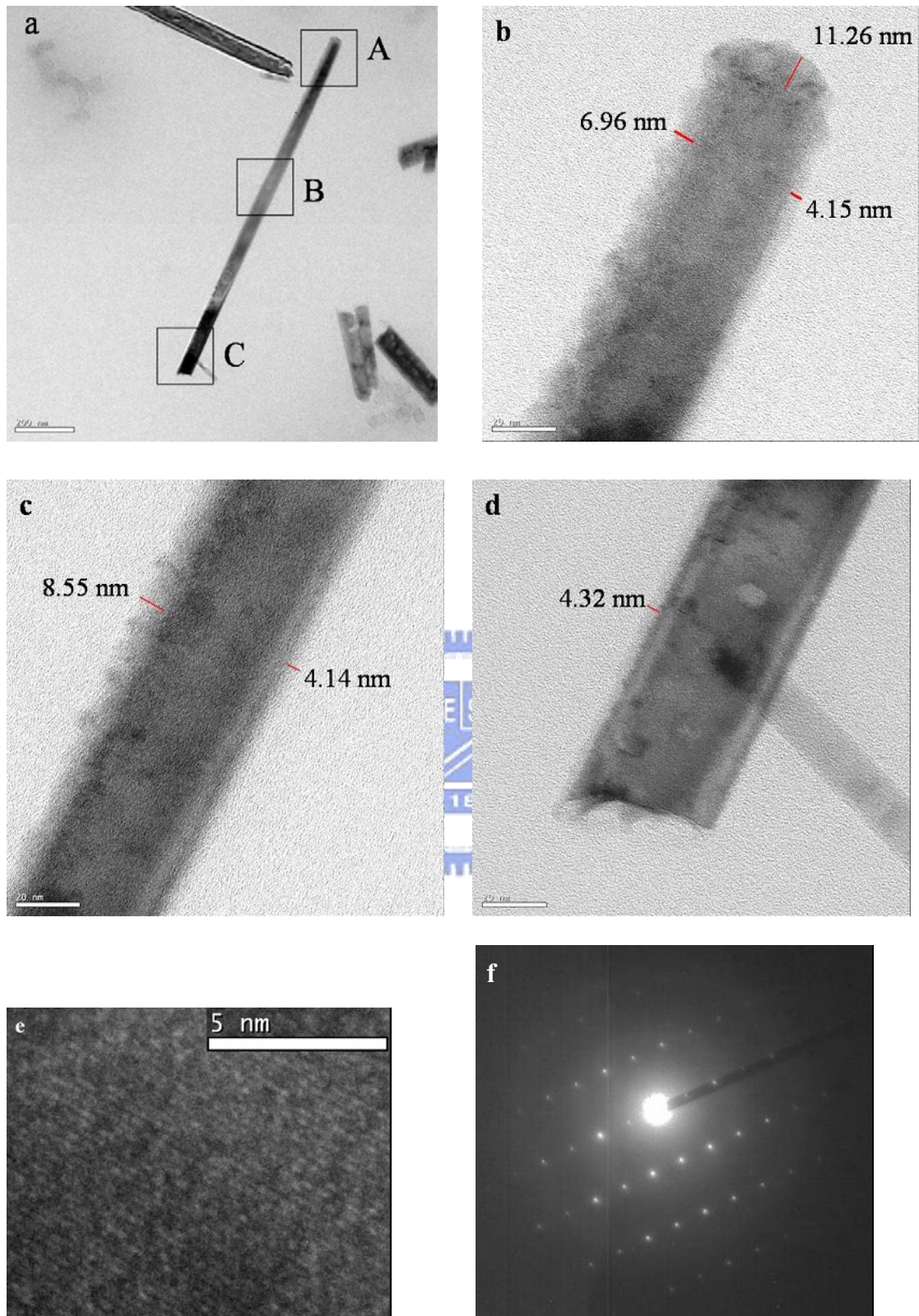


Figure 3-17. The TEM micrographs of (a) ZnO/TiO₂ core-shell structure. (b) region A (c) region B (d) region C. (e) The HR-TEM micrographs of region A (d) SAED spectra of region A.

	Zn	Ti	O
A	59.71%	10.03%	30.25%
B	71.96%	1.49%	26.55%
C	74.69%	1.41%	23.90%

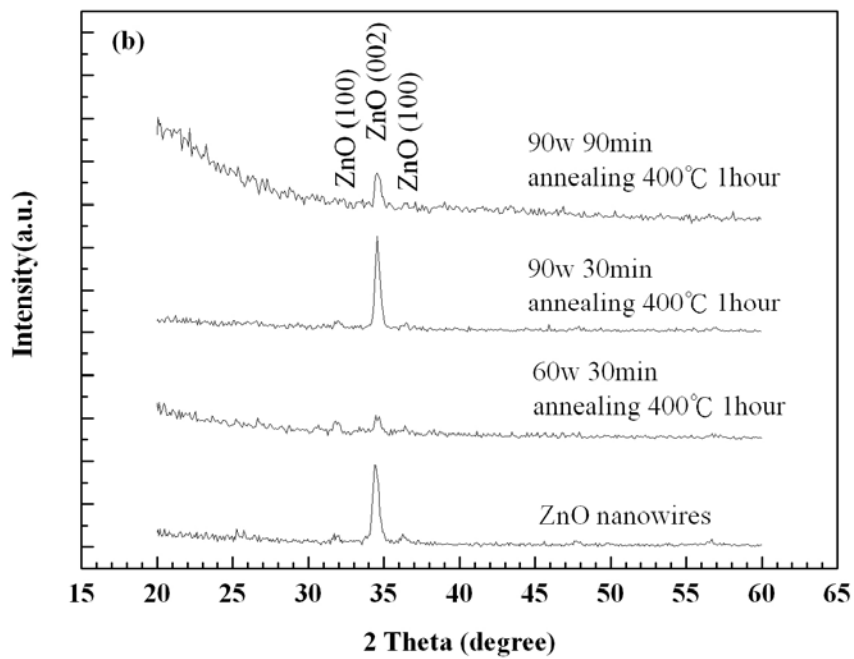
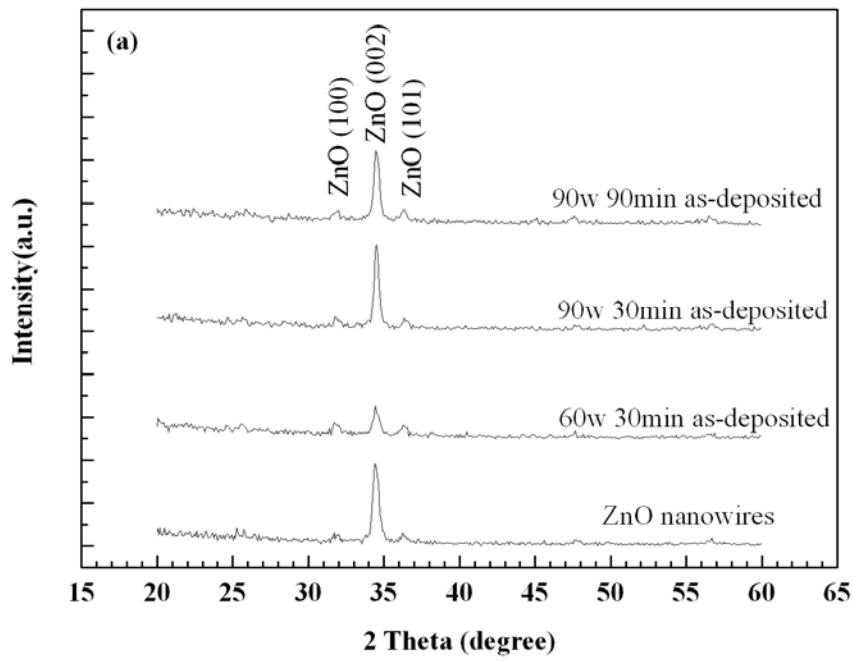
Table 3-2. The atomic percentage of ZnO/TiO₂ core-shell structure analyses by EDX.



3.3.3 The X-Ray Diffraction Analyses

Figure 3-18a shows the XRD patterns of ZnO/TiO₂ core-shell nanowires with various sputtering power, time as TiO₂ deposition. Figure 3-18b shows the XRD patterns of the structure with various sputtering power, time after annealing 400°C 1 hour in air. Figure 3-18c shows the XRD patterns of the structure with various sputtering power, time after annealing 500°C 1 hour in air.

From Figure 3-18a, it only show the peak at ZnO(100), ZnO(101) and ZnO(002). It means that ZnO nanowires are wurtzite and no other phase appear and TiO₂ shell on the ZnO nanowires is an amorphous type which are consistent with TEM analyses. From Figure 3-18b-c, it still did not appear any TiO₂ peak after annealing. Because of the lattice mismatch of wurtzite ZnO between Rtile and Aatase TiO₂, TiO₂ is hard to form any crystal structure on single crystalline ZnO nanowires. After the TiO₂ deposition, the ZnO(002) peak is somewhat a little shift form 34.300° to 34.502°. It means that the lattice constant of ZnO nanowres are changed. The small deviation of the lattice constants can be due to the lattice mismatch between TiO₂ and ZnO.



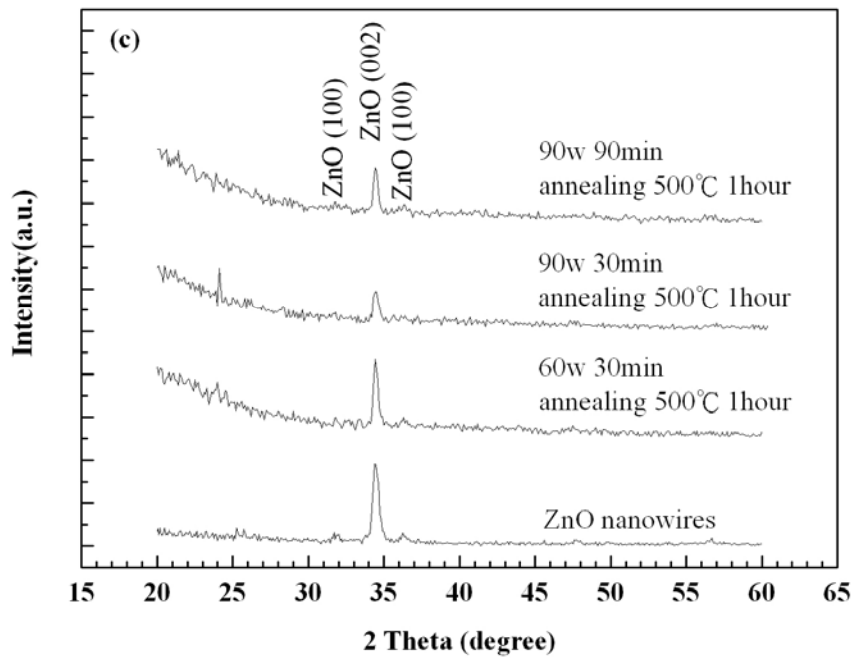


Figure 3-18. The XRD patterns of ZnO/TiO₂ core-shell structure with various sputtering power, time (a) as TiO₂ deposition, (b) after annealing 400°C 1 hour in air, (c) after annealing 500°C 1 hour in air.

3.3.4 The Optical Properties

Figure 3-19 shows the the cathodeluminescence (CL) spectra of ZnO nanowires and ZnO/TiO₂ core-shell structures as deposited. The ultraviolet (UV) emission peak (374 nm) of ZnO is generally attributed to the exciton-related activity, and the visible light region (450-700 nm) may be due to the transitions of native defects such as Zn vacancies, Zn interstitials, oxygen interstitials and single ionized oxygen vacancies. The imperfect boundaries and stacking faults of ZnO nanowires would cause the unstable surface states to trap impurities and further damage the optical property. Figure 3-19 show that the UV peak of ZnO/TiO₂ core-shell nanowires was stronger than the peak of ZnO nanowires and the visible light region emission of ZnO/TiO₂ core-shell structures became very weaker. It may be because that coating an amorphous TiO₂ film can repair the surface-related defects. Thus, the visible light region emission decreased so that the UV emission become stronger. In conclusion, coating TiO₂ film on ZnO is very important to improve the optical properties of ZnO.

In order to get better optical characteristic of ZnO, we put the ZnO/TiO₂ core-shell nanowires in the oven for thermal annealing 400°C and 500°C 1 hour under the air. Figure 3-20 show the CL spectras of ZnO/TiO₂ core-shell nanowires after thermal treatment. Unfortunately, the UV emission of ZnO/TiO₂ core-shell nanowires after thermal treatment was decreased and visible light region emission is increased. The green emission is commonly referred to a deep-level or a trap-state emission attributed to the singly ionized oxygen vacancy and the emission results from the radioactive recombination of photo-generated hole with an electron occupying the oxygen vacancy. The

visible light region emission may be because the nonstoichiometry TiO_2 attracted the oxygen in the ZnO nanowires in the thermal process. It will produce many single ionized oxygen vacancies (V_{O}^*) in the ZnO nanowires. Another reason is that after annealing Ti may diffuse into the ZnO nanowires. This phenomenon is resulted Zn vacancies (V_{Zn}), Zn interstitials (Zn_i), oxygen interstitials (O_i) and single ionized oxygen vacancies (V_{O}^*) in the ZnO nanowires. But the UV peak did not shift clearly and the ZnO(002) peak of XRD analyses is only a little shift. So that Ti may not diffuse into ZnO nanowires. Therefore, the main reason may be the nonstoichiometry TiO_2 . In conclusion, ZnO/ TiO_2 core-shell nanowires as deposited had best optical property.

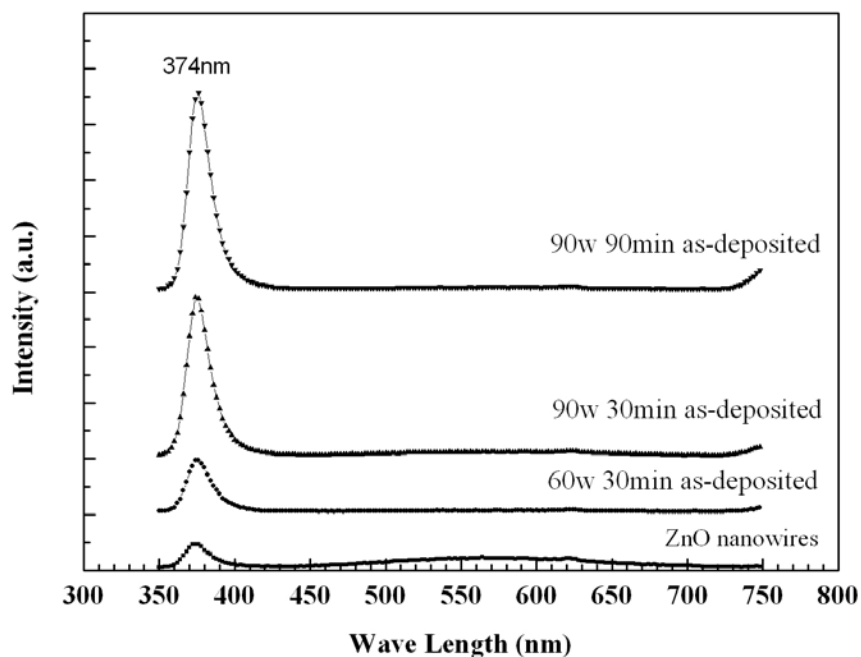


Figure 3-19. CL spectra of ZnO nanowires and ZnO/ TiO_2 core-shell nanowires as deposited.

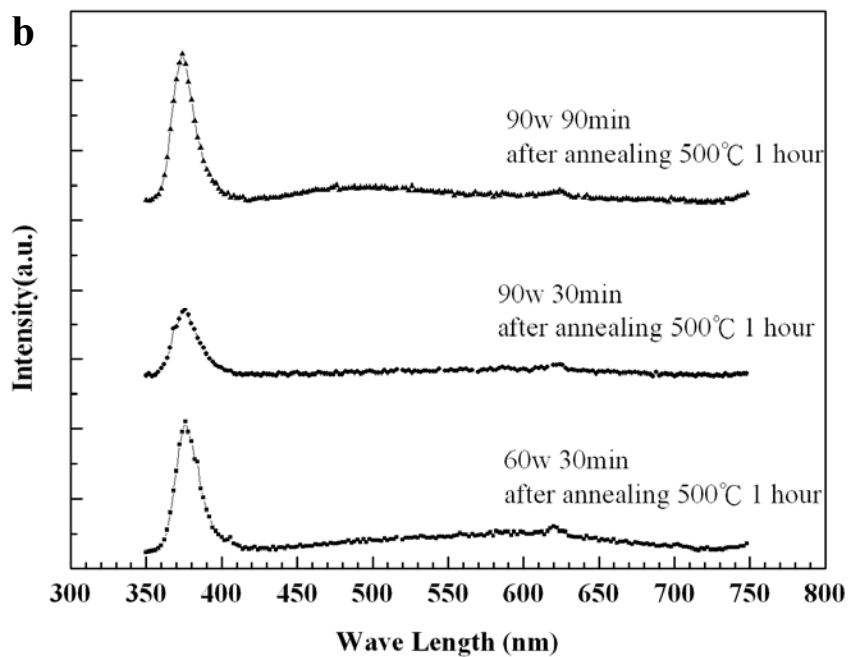
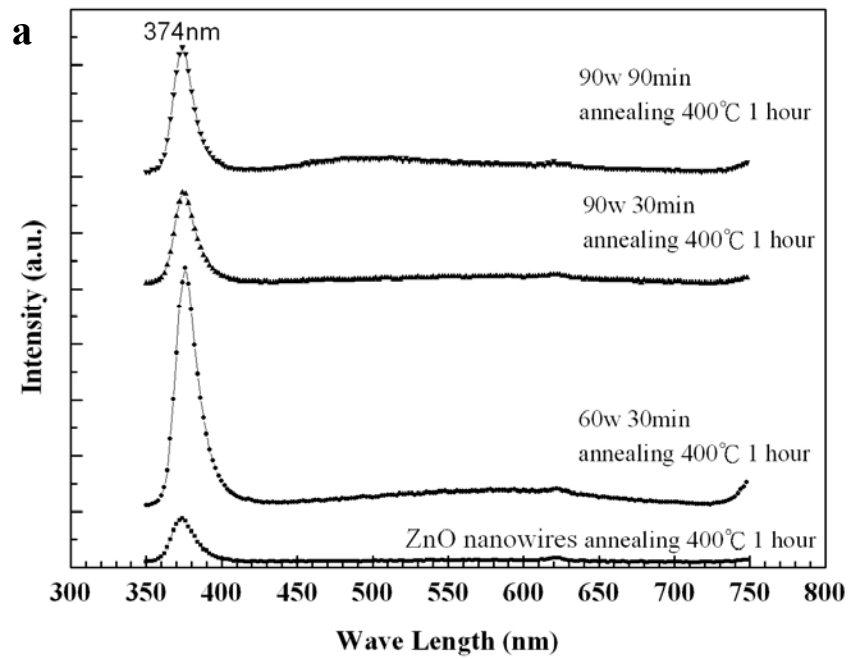


Figure 3-20. (a) CL spectra of ZnO nanowires and ZnO/TiO₂ core-shell nanowires after annealing 400°C (b) 500°C 1 hour under the air.

3.3.5 The Field Emission Properties

The field emission characteristics of ZnO/TiO₂ core-shell nanowires are indicated in Figure 3-22 and Table 3-3. Comparing with ZnO nanowires, ZnO/TiO₂ core-shell nanowires had higher E_{on} and lower β value. In addition, as the sputtered power and time increased, the turn on field increased. The reason may be that the nanowires with thicker TiO₂ film had lower aspect ratio. So that it is due to worse field emission properties. Another reason is that there is a barrier high at the interface between TiO₂ and ZnO as show in the Figure 3-21. The inter fields will let surface electron toward ZnO. It will let electrons pass through hardly so that nanowires needed a higher electric field to emit the electron. This phenomenon will reduce the field emission current and lower the β value. In other word, this phenomenon is an advantage of ZnO/TiO₂ core-shell nanowires which are used in DSSCs. The surface fields within each nanowire can be used to enforce charge separation and thereby ensure that faster transport results in a longer diffusion length in the nanowires.

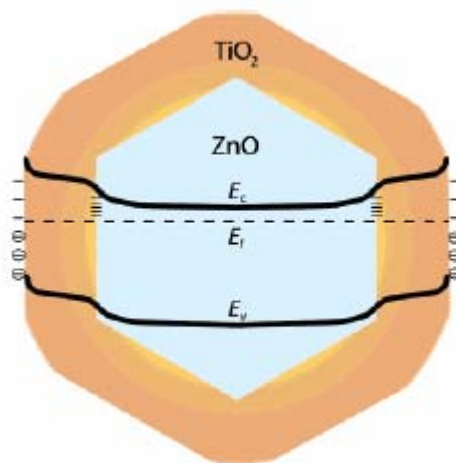


Figure 3-21. Schematic energy level diagram of a ZnO/TiO₂ core-shell structure.

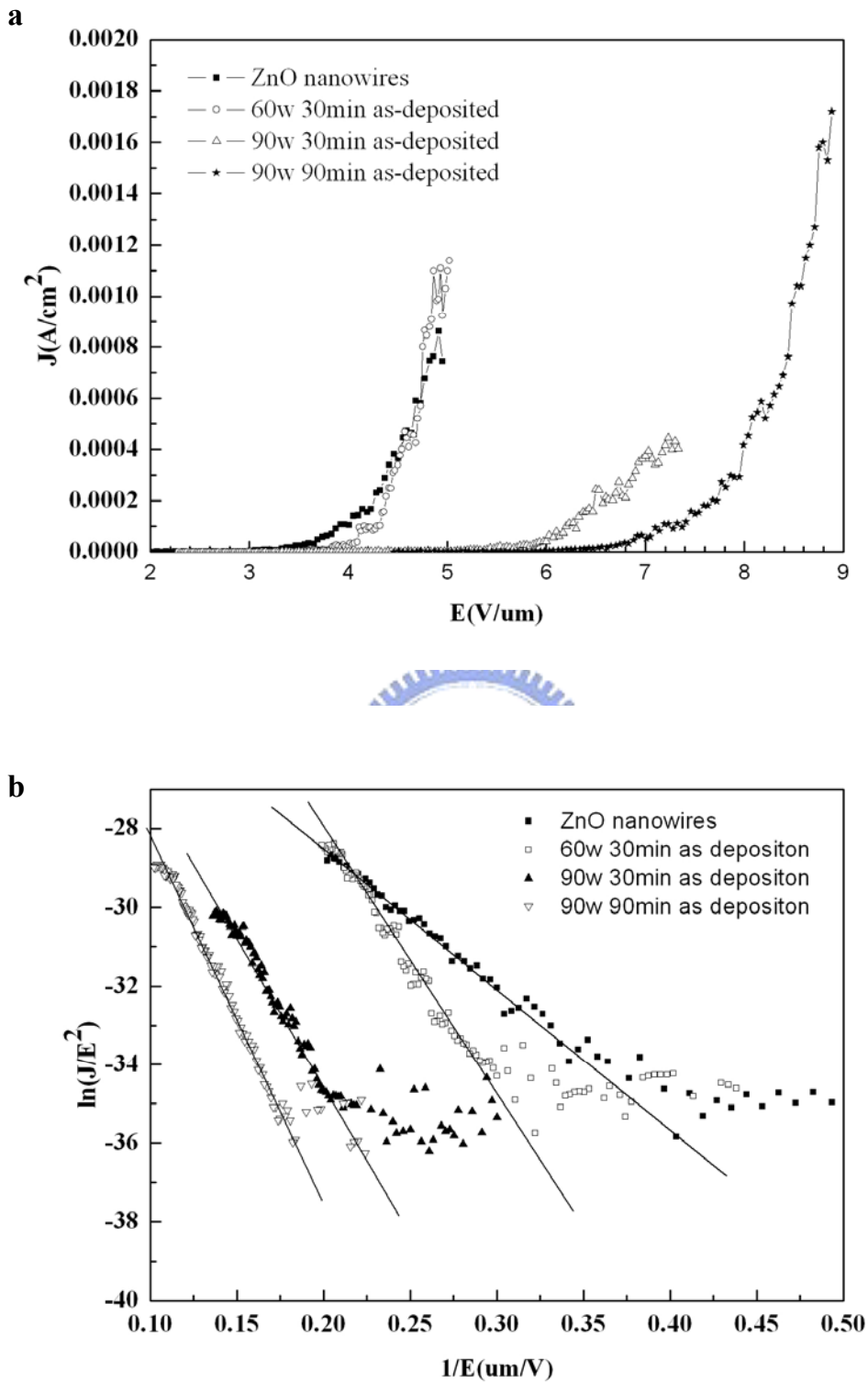
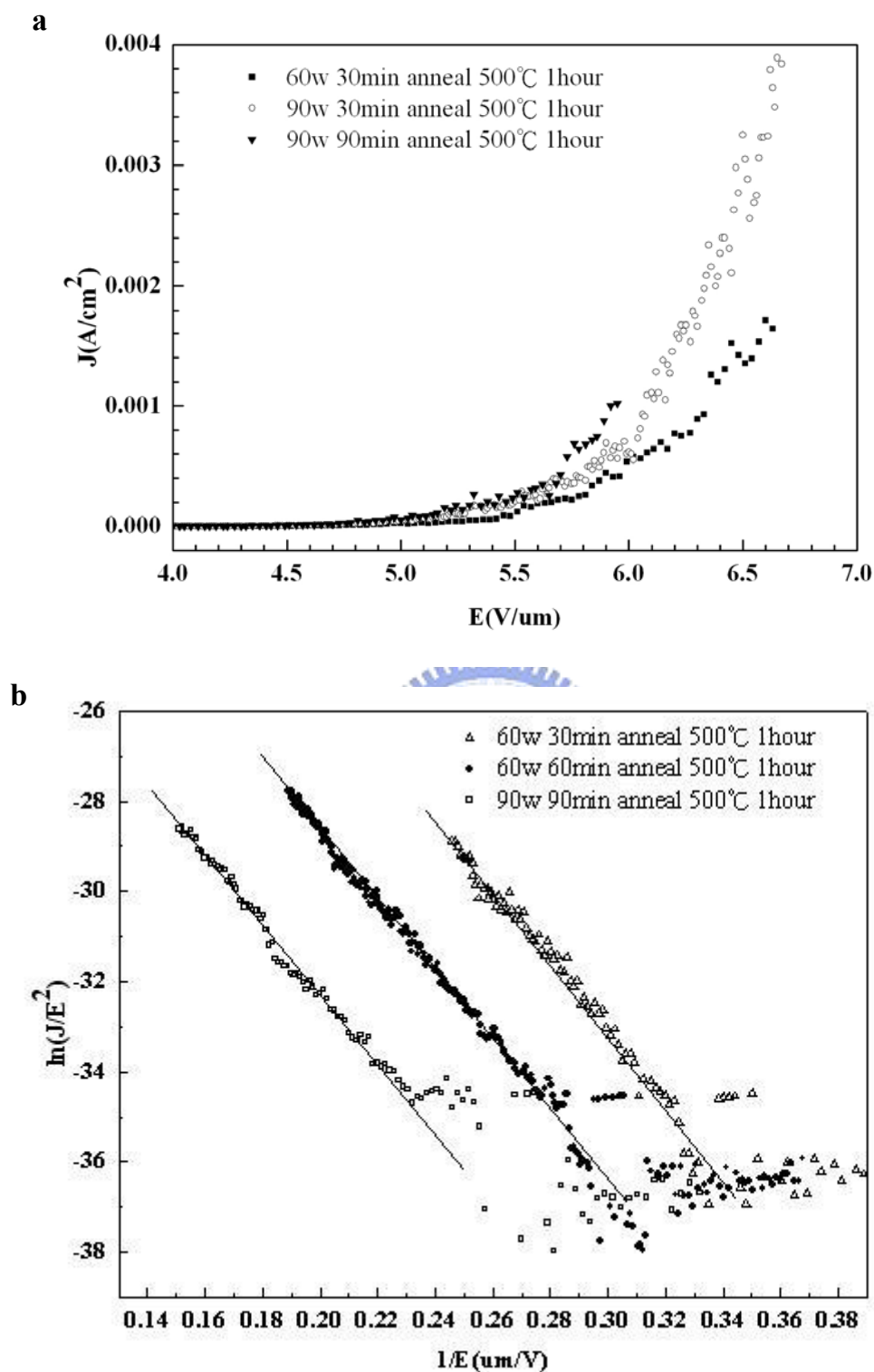


Figure 3-22. (a) Field emission current-voltage curves of ZnO/TiO₂ core-shell nanowires as deposited. (b) The F-N plot of ZnO/TiO₂ core-shell nanowires as deposited.

	ZnO nanowires	60w 30min as deposition	90w 30min as deposition	60w 60min as deposition	90w 90min as deposition
Electrode Area	0.00709(cm ²)	0.00709(cm ²)	0.00709(cm ²)	0.00709(cm ²)	0.00709(cm ²)
Work Function	5.37 eV (ZnO)	4.5 eV (TiO ₂)	4.5 eV (TiO ₂)	4.5 eV (TiO ₂)	4.5 eV (TiO ₂)
Eon	2.75 (V/μm)	3.01 (V/μm)	4.57 (V/μm)	4.59 (V/μm)	5.54 (V/μm)
Eth	x	4.86(V/μm)	x	6.98(V/μm)	x
Slope of F-N plots	34.47	64	76	85	95
β	2475.8	1023	861.64	492.3696	689.31

Table 3-3. The detail data of field emission property of ZnO/TiO₂ core-shell nanowires as deposited.

The field emission characteristics of ZnO/TiO₂ core-shell nanowires after thermal treatment are indicated in Figure 3-23. The detail data of field emission properties of ZnO/TiO₂ core-shell nanowires after annealing are indicated in Table 3-4. As the figures showed, the turn on fields and the field enhance factor of different sputtering conditions became similar. So aspect ratio is not the critical reason at this case. It is know from the CL analyses that there are many defects in the ZnO nanowires after annealing such as V_{Zn}, Zn_i, O_i and V_O* etc. The defects will catch the electrons and holes. Therefore, there is a large recombination current in the ZnO nanowires. This current will reduce the field emission current and the decrease the β value. So after thermal treatment the field emission characteristics of ZnO/TiO₂ core-shell nanowires are poorer.



	60w 30min after anneal 500°C 1hour	60w 60min after anneal 500°C 1hour	90w 90min after anneal 500°C 1hour
Electrode Area	0.00709(cm ²)	0.00709(cm ²)	0.00709(cm ²)
Work Function	4.5 eV (TiO ₂)	4.5 eV (TiO ₂)	4.5 eV (TiO ₂)
Eon	3.95 (V/μm)	3.90 (V/μm)	3.76 (V/μm)
Eth	6.36(V/μm)	6.08(V/μm)	5.92(V/μm)
Slope of F-N plots	80	76	75
β	818.56	861.64	873.13

Table 3-4. The detail data of field emission property of ZnO/TiO₂ core-shell nanowires after annealing.

3.4 TiO₂ Nanotubes

After the ZnO/TiO₂ core-shell nanowires complete, we put the samples in acetic acid (H₂O:CH₃COOH = 1000:1) for wet etching 30 min and 60 min. After wet etching 60 min, the ZnO seeding layer is dissolved in the solution and then the ZnO/TiO₂ core-shell nanowires float in the solution. So it is very hard to observe. After wet etching 30 min the ZnO seeding layer is still exist and the nanowires are still on the substrate. At the following section we only discussed the ZnO/TiO₂ core-shell nanowires after the wet etching 30 min.

3.4.1 The Field Emission Scanning Electron Microscopy

analyses

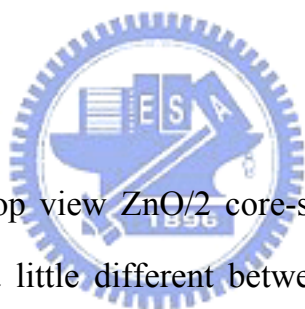


Figure 3-24a showed the top view ZnO/TiO₂ core-shell nanowires after the wet etching 30 min. There is a little different between after and before etching. After etching, some nanowires are lying on the substrate and some nanowires get together. They did not stand on the substrate straightly. It is because the seeding layer and some ZnO nanowires were etched by the acetic acid and there is no support in the TiO₂ shell. Furthermore, when the sample is taken out from the solution, the surface tension will bind nanowires together.

Figure 3-24b showed the cross section ZnO/TiO₂ core-shell nanowires after the wet etching 30 min. The great parts of TiO₂ shell are perfect, but there are some imperfect TiO₂ shells. It is because that some ZnO nanowires did not stand on the substrate straightly. And then, TiO₂ can not coat full around on those lopsided nanowires at the sputtering process. Thus, after etching those shells showed the imperfect part at the tube end.

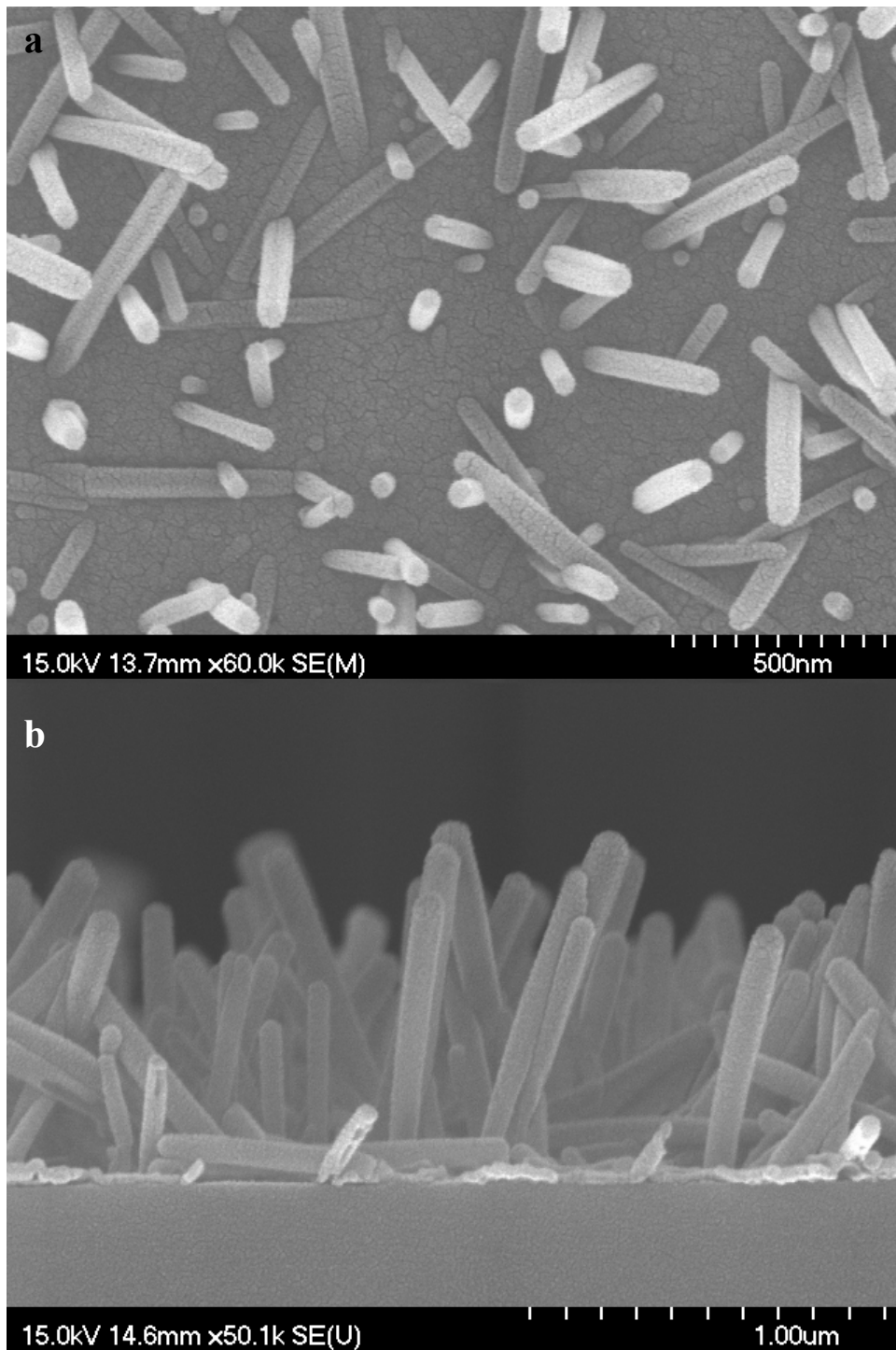
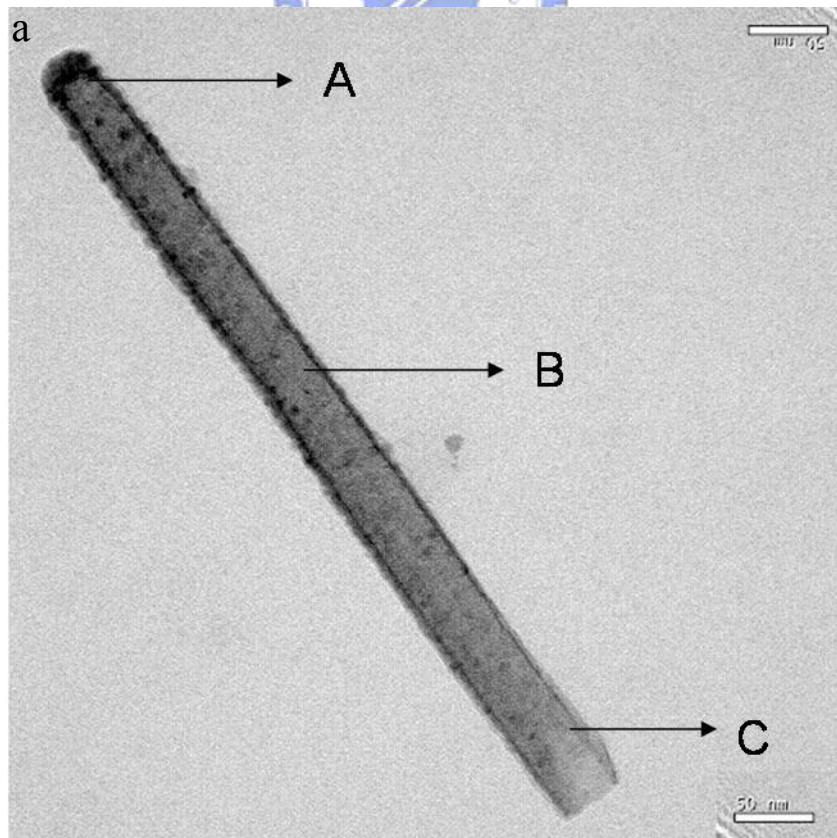


Figure 3-24. The SEM image of ZnO/TiO₂ core-shell nanowires after wet etching 30 min (a) top view (b) cross section.

3.4.2 The High Resolution Transmission Electron

Microscopy Analyses and Dispersive X-Ray Energy

Figure 3-25a showed the TEM image of TiO₂ tube. Figure 3-25b showed the high resolution image of the region B. The uniform diameter, length of the tube is 44.29 nm, 579.69 nm respectively. The TiO₂ shell is 6.26 nm and 8.08 nm at right and left side. Figure 3-25c showed the SAED pattern of TiO₂ tube. It showed that there was no single crystalline structure in this tube clearly and the TiO₂ was amorphous. The result is the same as the XRD. Table 3-5 showed the composition of the tube which is analyzed by the EDX. It reveals that Zn (1.19 %) and Ti (98.81 %) at the top; Zn (3.61 %) and Ti (96.39 %) at the middle; Zn (6.83 %) and Ti (93.17 %) at the end. All the evidences indicated there is a hollow nanotube. In other words, the TiO₂ can coat on the ZnO nanowires at less 550 nm.



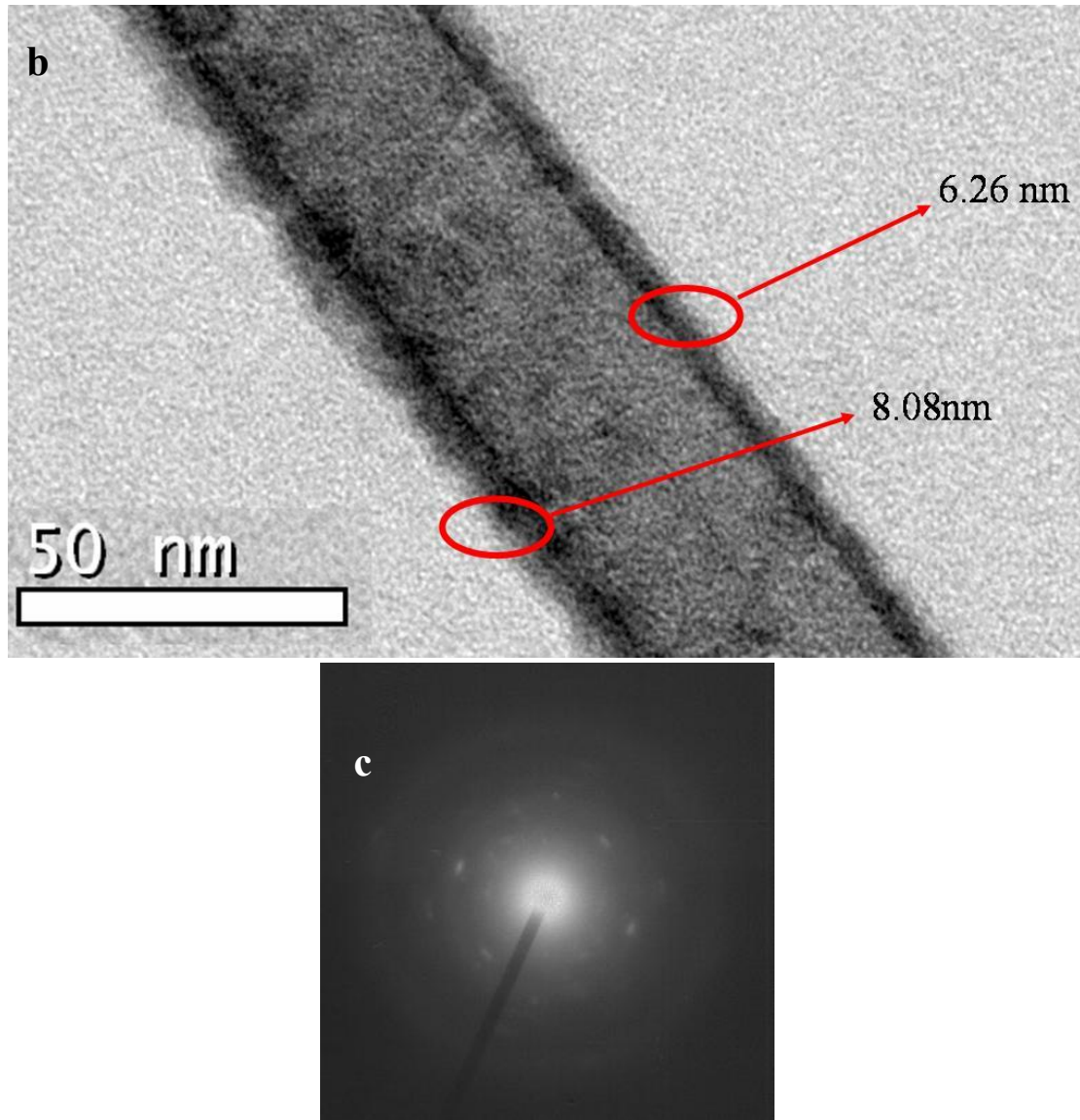


Figure 3-25. The TEM micrographs of (a) TiO₂ tube. (b) region B (c) SAED spectra of region B.

	Zn	Ti
Region A	1.19 %	98.81 %
Region B	3.61 %	96.39 %
Region C	6.83 %	93.17 %

Table 3-5. The atomic percentage of ZnO/TiO₂ core-shell structure analyses by EDX.

Figure 3-26a showed the TEM image of ZnO/TiO₂ nanowires. Figure 3-26b showed high resolution image of region C. From the Figure 3-26a, ZnO is still residual in the TiO₂ shell after wet etching. The diameter and length of this nanowire are about 54 nm and 651.5 nm, respectively. From the Figure 3-26b the TiO₂ shell is about 3.44 nm and 5.94 nm. Figure 3-27a-b showed the SAED pattern of region B and C. It showed the there are ZnO nanowire and TiO₂ shell at the region C. The ZnO nanowire is single crystalline with wurtzite and TiO₂ is amorphous type at region B. Figure 3-27 showed the TiO₂ shell is amorphous at the region C. Table 3-6 showed the atomic percentage of this nanowire. There are a large percentage of atomic at region A and region B. It impaled that there is ZnO under the TiO₂ shell. In the other words, the ZnO nanowrie is not etched completely after etching 30 min.



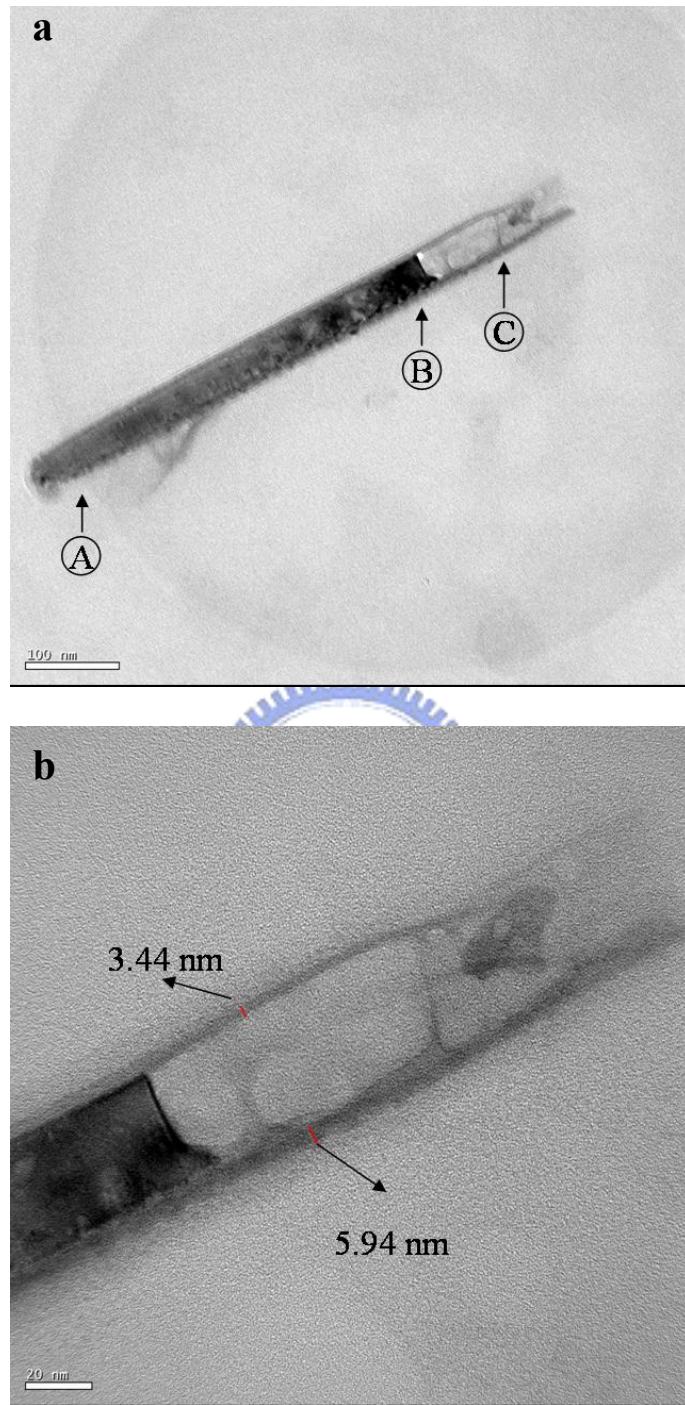


Figure 3-26. The TEM micrographs of (a) ZnO/TiO₂ nanowire. (b) region B.

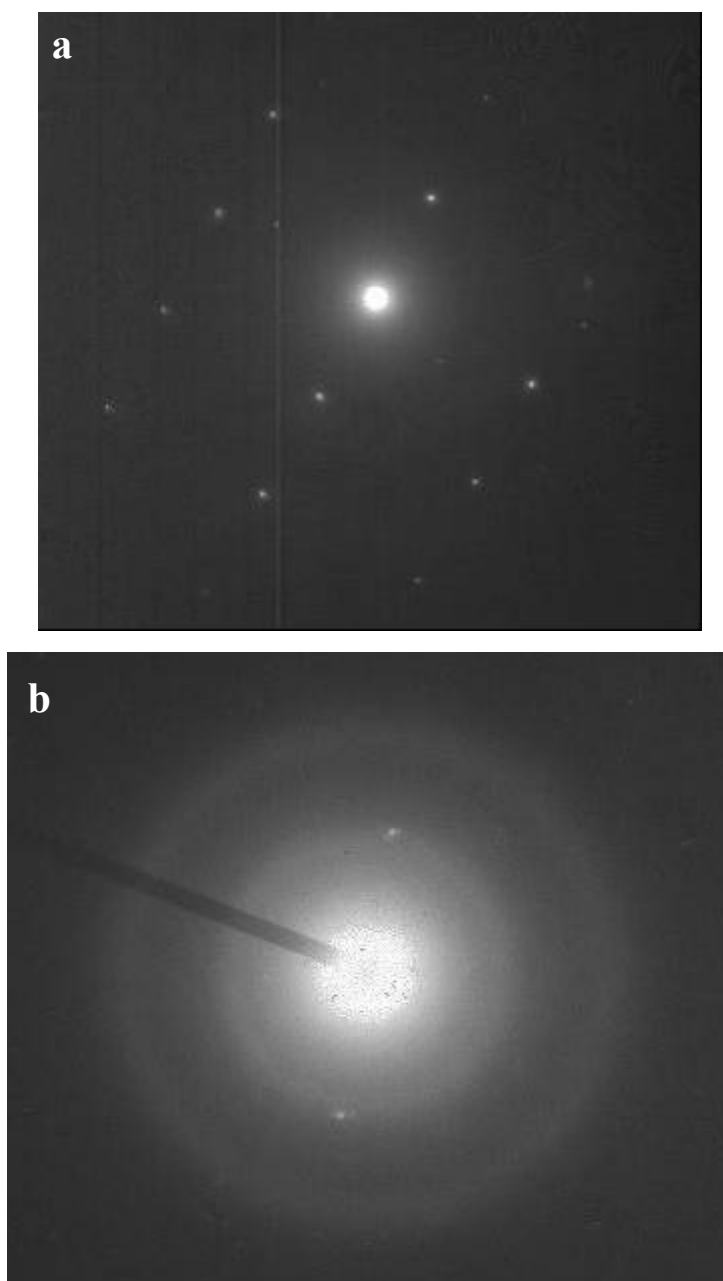


Figure 3-27. SAED spectra of (a) region B (b) region C.

	Zn	Ti
Region A	84.13 %	15.87 %
Region B	90.9 %	9.10 %
Region C	38.46 %	61.54 %

Table 3-6. The atomic percentage of ZnO/TiO₂ core-shell structure analyses by EDX.

Chapter 4 Conclusions

In summary, the hydrothermal method provides the simple, environmental friendliness, low cost and low temperature (below 100°C) way to grow ZnO nanowires. The ZnO/TiO₂ core-shell nanowires and TiO₂ tubes can be fabricated by the sputtering method and simple wet etching process.

As the concentration of the chemical solution increases, the aspect ratio of ZnO nanowires decreased. As the growth time increases, the lengths of the ZnO nanowires increase.

After the TiO₂ coating on the ZnO nanowires the optical properties were improved. The UV emission became very strong and visible emission became very weak. After the thermal treatment, the UV emission became very weaker and visible emission became very stronger. It may be because of the nonstoichiometry TiO₂ attract the oxygen from the ZnO nanowires during the thermal process. The phenomenon produced many single ionic oxygen vacancies in the ZnO nanowires and impaired the optical properties.

After TiO₂ coating, the field emission characteristic will change. The turn on field increased and the β value decreased. It may be because that the nanowires with thicker TiO₂ film has lower aspect ratio. Another reason is that there is a barrier high at the interface between TiO₂ and ZnO. The inter field will let the electron pass through hardly and nanowires needed a higher electric field to emission. After the thermal treatment, there will be many defects in the ZnO. And the defect will catch the electron and become a recombination current in the ZnO nanowires so that it reduced the field emission current.

In other word, the field between ZnO and TiO₂ is an advantage of using in

dye-sensitized solar cells. The surface fields within each nanowire can be used to enforce charge separation and thereby ensure that faster transport results in a longer diffusion length in the nanowires.



Reference

- ¹ Q. B. Wu, S. Ren, S. Z. Deng, J. Chen, and N. S. Xu *J. Vac. Sci. Technol.* B22(3),1282 (2004).
- ² P. L. Chen, J. K. Chang, C. T. Kau, and F. M. Pan, *Appl. Phys. Lett* 86, 123111 (2005).
- ³ K. H. Jung, J. W. Yoon, N. Koshizaki and Y. S. Kwon *Jpn. J. Appl. Phys.* 44, 7A 5300 (2005).
- ⁴ S. H. Jeong and K. H. Lee *Jpn. J. Appl. Phys* 8B, L1106 (2004).
- ⁵ H. O. Le and S. J. Chua, Y. W. Koh and K. P. Loh, Z. Chen, C. V. Thompson and E.A. Fitzgerald *Appl. Phys. Lett* 87, 101908 (2005).
- ⁶ Y. F. Mei, Z. M. Li, R. M. Chu, and Z. K. Tang, G. G. Siu, Ricky K. Y. Fu, and Paul K. Chu, W. W. Wu and K. W. Cheah *Appl. Phys. Lett* 86, 021111 (2005).
- ⁷ Y. B. Tang, H. T. Cong, Z.G. Zhao, and H. M. Cheng *Appl. Phys. Lett* 86, 153104 (2005).
- ⁸ H. Hu, K. Yu, J. Zhu, Z. Zhu. *Applied Surface Science* 252, 8410–8413 (2006).
- ⁹ B. Cao, W. Cai, Y. Li, F. Sun and L. Zhang, *Nanotechnology* 16, 1734 (2005).
- ¹⁰ C. L. Kuo, T. J. Kuo, and M. H. Huang *J. Appl. Chem. B* 109,20115 (2005).
- ¹¹ F. Xu, K. Yu, G. Li, Q. Li and Z. Zhu, *Nanotechnology* 17, 2855–2859 (2006).
- ¹² M. H. Liao, C. H. Hsu, D. H. Chen, *Journal of Solid State Chemistry* 179, 2020–2026 (2006).

-
- ¹³ Q. Kuang, Z. Y. Jiang, Z. X. Xie, S. C. Lin, Z. W. Lin, S. Y. Xie, R. B. Huang, and L. S. Zheng *J. AM. CHEM. SOC.* **127**, 11777-11784 (2005)
- ¹⁴ S. Iijima, *Nature (london)* **354**,56 (1991).
- ¹⁵ C. Agashe, O. Kluth, J. Hupkes, U. Zastrow, B. Rech and M. Wuttig, *J. Appl. Phys.* **85** 1911 (2003)
- ¹⁶ H. Cao, Y. G. Zhao, H. C. ONg, S. T. Ho, J. Y. Dai, J.Y. Wu and R. P. H. Chang, *Appl. Phys. Lett.* **73** 3656 (1998).
- ¹⁷ S. Y. Li, P Lin, C. Y. Lee and T. Y. Tseng, *J. Appl. Phys.* **95** 3711 (2004)
- ¹⁸ R. S. Wagner and W. C. Ellis, *Appl. Phys. Lett.* **4**,89 (1964).
- ¹⁹ G. Shi, C.M. Mo, W.L. Cai, L.D. Zhang , *Solid State Communications* **115** 253-256 (2000)
- ²⁰ C. Y. Lee, T. Y. Tseng, S. Y. Li and P. L., *Nanotechnology* **17**, 83–88 (2006)
- ²¹ C. Y. Lee, T. Y. Tseng, S. Y. Li and P. L., *Nanotechnology* **16**, 1105–1111 (2005).
- ²² C. Y. Lee, T. Y. Tseng, S. Y. Li and P. L., *J. Appl. Phys.* **99**, 024303 (2006).
- ²³ K. Vanheusden, W.L. Warren, C.H. Seager, D.R. Tallant, J.A. Voigt and B. E. Gnade, *J. Appl. Phys.* **79**,7983 (1996) .
- ²⁴ K. Vanheusden, W. L. Warren, C. H. Seager, D. R. Tallant, and J. A. Voigt B. E. Gnade, *J. Appl. Phys.* **79**, 7983-7990 (1996).
- ²⁵ K. Vanheusden, W.L. Warren, C.H. Seager, D.R. Tallant, J.A. Voigt, B.E. Gnade, *J. Appl. Phys.* **79**, 7983 (1996).
- ²⁶ C. Kim, A. Park, K. Prabakar, C. Lee, *Materials Research Bulletin* **41**, 253–259 (2006).
- ²⁷ A. Poëppl and G. Voëlkel, *Phys. Status Solidi A* **125**, 571 (1991).
- ²⁸ E. Francisco; M. Bermejo, V. Baonza Garcia, L. Gerward, JM. Recio, *Phys. Review B* **67** (6), 064110-1 (2003).

-
- ²⁹ C. Feldmann, *Adv. Mater.* 13, 1301-1303.(2001)
- ³⁰ M. Anpo; T. Shima; S. Kodama; Y. Kubokawa, *J. Phys. Chem.* 91, 4305-4310 (1987).
- ³¹ O'Regan, B.; Gratzel, M. *Nature* 353, 737-740 (1991).
- ³² J. M. Wu, H. C. Shih , W.T. Wu, *Chem. Phys. Lett.* 413 490–494 (2005).
- ³³ D. Chen, J. Liu, P. Wang, L. Zhang, J. Ren, F. Tang and W. Wu ,*Colloids and Surfaces A: Physicochem* 302, 461–466 (2007).
- ³⁴ F. Caruso, *Adv. Mater.* 13 11–22 (2001).
- ³⁵ M. Law, L. E. Greene, A. Radenovic, T. Kuykendall, J. Liphardt, and P. Yang, *J. Phys. Chem. B* 110, 22652-22663 (2006).
- ³⁶ J.B. Jackso, N.J. Halas, Silver nanoshells, *J. Phys. Chem. B* 105 2743–2746 (2001).
- ³⁷ C. Graf, A. van Blaaderen, *Langmuir* 18, 524–534 (2002).
- ³⁸ S.A. Kalele, S.S. Ashtaputre, N.Y. Hebalkar, S.W. Gosavi, D.N. Deobagkar, D.D. Deobagkar, S.K. Kulkarni, *Chem. Phys. Lett.* 404, 136–141 (2005).
- ³⁹ S. Y. Li, C. Y. Lee, T. Y. Tseng, *J. Cryst. Growth* 247, 357 (2003).